B cells specific for polyomavirus-derived oncoprotein are predictive of Merkel cell carcinoma progression

Authors:
Haroldo J. Rodriguez[1,3,4,5,10], Allison J. Remington[4], Matthew D. Gray[3], Rian Alam[4], Macy W. Gilmour[4], Carina Morningstar[4], Gabriel F. Alencar[1,2], Thomas Pulliam[4], Erin McClure[4], Neha Singh[4], Francesca Urselli[3], Katrina Poljakov[3], Kimberly Smythe[9], Rima Kulikauskas[4], Kristin L. Robinson[9], Ata S. Moshiri[14], Cecilia C.S. Yeung[9,10], Minggang Lin[9], Kristen Shimp[9], Allison Schwartz[3], Anne M. Macy[3], Marti R. Tooley[3], Melissa L. Baker[3], Joseph J. Carter[8], Kayla Hopwo[9], Naina Singhi[9], Jakob Bakhtiari[9], Mikel Ruterbusch[9], Carolyn Shasha[3], Maria Iuliano[9], Logan J. Mullen[3], Blair L. DeBuysscher[3], Joshua R. Veatch[9], David M. Koelle[10,11,12,13], Denise A. Galloway[8], Paul Nghiem[4,6,*], Justin J. Taylor[1,2,3,7,*]

Affiliations:
[1]Beirne B. Carter Center for Immunology Research, University of Virginia, Charlottesville, VA, USA.
[2]Division of Infectious Disease and International Health, Department of Medicine, University of Virginia, Charlottesville, VA, USA.
[3]Vaccine and Infectious Disease Division, Fred Hutchinson Cancer Center, Seattle, WA, USA
[4]Department of Dermatology, University of Washington, Seattle, WA, USA
[5]Molecular Medicine and Mechanisms of Disease PhD Program, University of Washington, Seattle, WA, USA
[6]Department of Immunology, University of Washington, Seattle, WA, USA
[7]Department of Microbiology, Immunology, and Cancer Biology, University of Virginia, Charlottesville, VA, USA.
[8]Human Biology Division, Fred Hutchinson Cancer Center, Seattle, WA, USA.
[9]Translational Science and Therapeutics Division, Fred Hutchinson Cancer Center, Seattle, WA, USA.
[10]Department of Laboratory Medicine and Pathology, University of Washington, Seattle, Washington.
[11]Department of Medicine, Division of Allergy and Infectious Diseases, University of Washington, Seattle, Washington.
[12]Department of Global Health, University of Washington, Seattle, WA, USA
[13]Benaroya Research Institute, Seattle, WA, USA
[14]Ronald O. Perelman Department of Dermatology, New York University Grossman School of Medicine, New York, NY, USA

*Contributed equally & correspondence to: justintaylor@virginia.edu, pnghiem@uw.edu

Abbreviations:
APC, allophycocyanin; **APC755**, APC-DyLight 755; **ASC**, antibody-secreting cell; **AUC**, area under the curve; **BLI**, Bio-Layer Interferometry; **CFA**, complete Freund's adjuvant; **CITEseq**, Cellular Indexing of Transcriptomics and Epitopes by Sequencing; **CLL**, Chronic Lymphocytic Leukemia; **GST**, glutathione S-transferase; **HPV**, Human Papillomavirus; **Ig**, immunoglobulin; ***IgH***, antibody heavy chain gene; ***IgL***, antibody light chain gene; **LN**, lymph node; **MCC**, Merkel cell carcinoma; **MCL**, Mantle Cell Lymphoma; **MCPyV**, Merkel cell polyomavirus; **mIHC**, multiplex immunohistochemistry; **PBMC**, peripheral blood mononuclear cells; **PE**, R-phycoerythrin; **PE594**, PE-DyLight 594; **PE650**, PE-DyLight 650; **RSV**, Respiratory Syncytial Virus; **T-Ag**, T-antigen; **TCR**, T cell receptor; **T_{FH}**, follicular helper $CD4^+$ T cell; **UMAP**, uniform manifold approximation and projection.

Abstract

Merkel cell carcinoma often results from integration of a truncated version of the Merkel cell polyomavirus. This leads to expression of immunogenic viral oncoproteins that promote tumorigenesis. While the importance of viral oncoprotein-specific T cells in anti-MCC immunity is well established, the roles B cells play in MCC control have not been explored. Here, we analyzed the frequency and phenotype of viral oncoprotein-specific and total B cells from MCC patient blood and tumors. Strikingly, although no blood-associated B cell phenotypes strongly correlated with disease outcome, detection of oncoprotein-specific antibody-secreting and/or germinal center B cells in MCC tumors accurately predicted disease control. *In vitro*, B cells engineered to be specific for viral oncoproteins induced robust activation of oncoprotein-specific CD4+ T cells. Together, our findings suggest that cancer-specific B cells could promote anti-tumor immunity via increased T cell responses and that approaches to augment cancer-specific B cell function could benefit MCC patients.

Statement of Significance

The link between cancer-specific B cells in anti-tumor immunity and clinical outcomes remains poorly defined. Here, we show that tumor-associated B cells specific for a viral oncoprotein expressed in MCC patient tumors predict disease control with remarkable accuracy, establishing their potential as active participants in tumor immunity.

Running title

Cancer-specific B cells in MCC predict disease outcomes.

Keywords

B cells, T cells, cancer, Merkel cell carcinoma, tumors.

Introduction

Merkel cell carcinoma (MCC) is a rare aggressive skin cancer with a mortality rate of ~30%[1-4]. MCC is usually driven by integration of Merkel cell polyomavirus (MCPyV) T-antigen (T-Ag) DNA into host chromosomes. This leads to constitutive expression of the viral small and truncated large T-Ag oncogenic proteins responsible for tumorigenesis[5-7]. T-Ag oncoproteins are immunogenic and targeted by T cells[8-11] and B cells[12,13]. While studies have established the importance of MCPyV T-Ag-specific $CD8^+$ T cells in MCC tumor control, the role that antibodies and B cells play in anti-tumor immunity is unknown.

Most patients with T-Ag-driven MCC have T-Ag-specific antibodies in blood that are largely undetectable in individuals without MCC[12,13]. The level of T-Ag-specific antibodies at the time of diagnosis is correlated with tumor burden but are not predictive of MCC progression after tumor surgical excision and local radiation[12,13]. In people that do not experience MCC progression, the level of T-Ag-specific antibodies declines rapidly, often becoming undetectable. In contrast, stable levels of T-Ag-specific antibodies or a brief decline followed by rapid increase usually indicates MCC progression[12-14]. These dynamics combined with the intracellular expression of T-Ag have led to a model where T-Ag-specific antibodies are produced in response to the presence of MCC but do not play a role in tumor control.

Addressing the function of tumor-specific B cells is challenging due to the diversity in tumor antigens which often varies from person-to-person even amongst cancers of the same type[15,16]. Studying tumor-specific B cell responses is further complicated by their low frequency in solid tumors[17-19]. Animal studies have demonstrated that cancer-specific B cells can enhance anti-tumor immunity by promoting antigen presentation to $CD4^+$ T cells, which in turn can recruit and enhance cancer-specific $CD8^+$ T cells to the tumor microenvironment[20]. Interestingly, tumors from Human Papillomavirus $(HPV)^+$ head and neck cancer patients contain HPV-specific B cells [21,22], but whether or not these cells contribute to HPV tumor control or associate with disease outcomes is not known.

Expression of T-Ag oncoproteins by MCC allows for study of cancer-specific B cell responses across patients using T-Ag tetramers. We find that while T-Ag-specific B cells are found at increased frequencies in the blood of MCC patients compared to controls, phenotypes did not associate with disease outcome. In contrast, detection of T-Ag-specific antibody-secreting and/or germinal center B cells in tumor samples is predictive of extended progression-free survival after treatment, whereas low or undetectable levels of these cells predicted rapid MCC progression. Using antibodies and T cell receptors (TCR) identified from patient samples to engineer human T-Ag-specific B cells and $CD4^+$ T cells, we demonstrate highly efficient cognate antigen presentation, suggesting a mechanism by which local specific B cells can enhance T cell-mediated immunity. Together these findings show the predictive power of local T-Ag-specific B cells as biomarkers of MCC control and suggest that functional B cell responses promote anti-tumor immunity by facilitating antigen-presentation to T cells.

Results

Validation of T-Ag protein tetramers to detect T-Ag-specific B cells.

To identify T-Ag-specific B cells using flow cytometry, fluorescent T-Ag tetramers were used in combination with control tetramers[23,24] to exclude B cells specific for streptavidin, the fluorochrome, and the glutathione S-transferase (GST) purification tag added to T-Ag. We used the common domain shared by small and large T-Ag isoforms since this domain is rarely mutated from patient-to-patient and most T-Ag-specific serum antibodies appear to target this region[12,25]. In contrast, the large T-Ag varies from patient-to-patient as a protein ranging from 228 - 778 amino acids depending upon the location of truncation[25-28]. Therefore, use of a tetramer only containing the “common” T-Ag domain[29,30] allowed direct comparison of B cells binding the same antigen across cohorts. As done previously[23,24], rare tetramer-binding B cells were more easily assessed when enriched using anti-fluorochrome microbeads before analysis. To validate the T-Ag tetramer, we immunized mice with T-Ag in complete Freund’s adjuvant (CFA) and found a robust expansion of T-Ag tetramer-binding live B cells compared to control animals injected with CFA alone (**Figure 1a, b**). Antibody-secreting cells and germinal center B cells

were also present within this expanded population in T-Ag/CFA injected animals but absent in control animals (**Figure 1c**).

We next assessed T-Ag tetramer-binding B cells from the blood of patients with progressive T-Ag-driven MCC and control individuals with no history of MCC (**Figure 1d, e**). Single cells were sorted into individual wells of a 96-well plate and paired heavy and light chain sequences were determined using RT-PCR (**Table S1**). From these sequences five antibodies were produced from control samples and five from MCC samples. In total, 8/10 antibodies were confirmed to bind T-Ag using Bio-Layer Interferometry (BLI) indicating high specificity of the tetramer-based approach (**Figure 1f, g**).

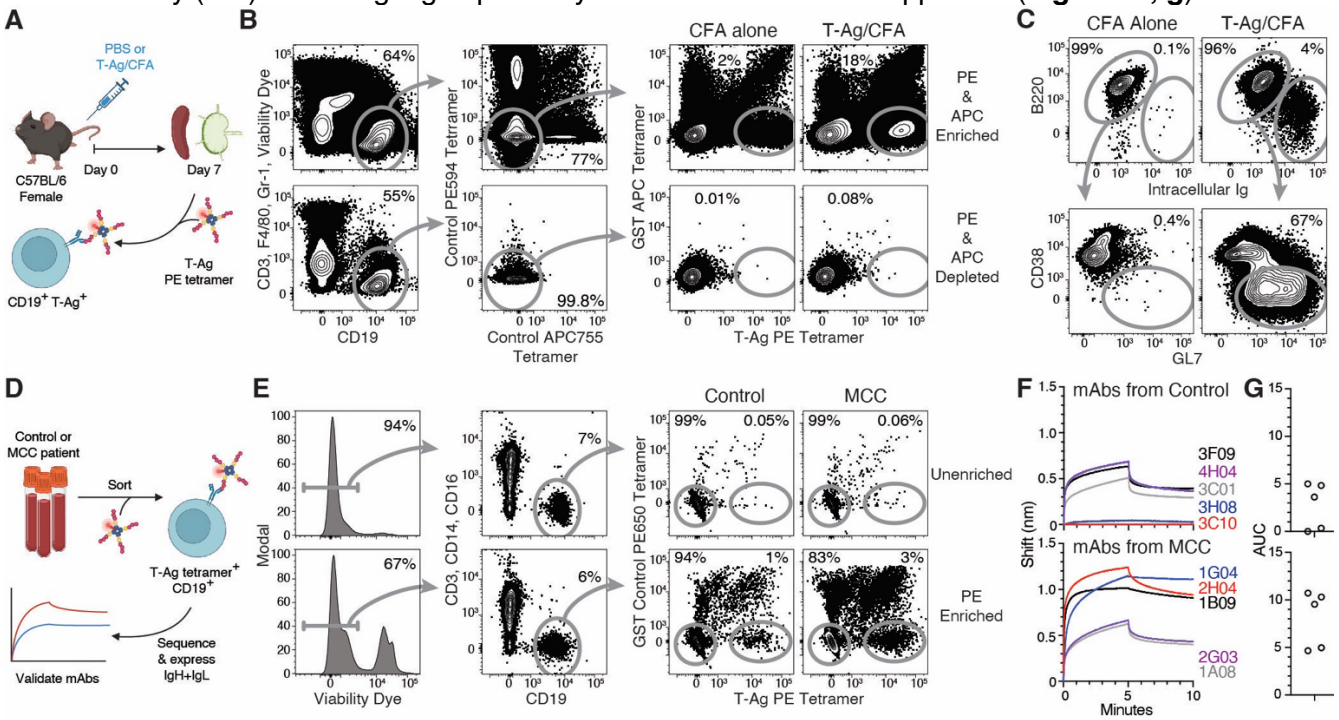

Figure 1. Detection of T-Ag-specific B cells in patient blood using T-Ag tetramers. **A**. Schematic representation of two experiments used to validate identification of T-Ag-specific mouse B cells using T-Ag tetramers. **B**. Representative flow cytometry of live CD19$^+$ B220$^+$ CD3$^-$ Gr-1$^-$ F4/80$^-$ B cells binding T-Ag PE tetramers but not GST APC control tetramers, PE594 control tetramers or APC755 control tetramers in samples from mice seven days after subcutaneous injection of 5 μg of T-Ag in CFA in the base of the tail with compared to control mice injected with CFA alone. Each sample was enriched with anti-PE and anti-APC microbeads prior to analysis and both the PE/APC-enriched and -depleted fractions are displayed. **C**. Representative flow cytometry of T antigen tetramer-binding B220^{LOW} Ig^{++} antibody-secreting cells and GL7$^+$ CD38$^-$ B220$^+$ Ig$^+$ germinal center B cells from mice seven days after subcutaneous injection of 5 μg of T-Ag in CFA in the base of the tail compared to uninjected control mice. **D**. Schematic representation of an experiment used to validate identification of T-Ag-specific human B cells using T-Ag tetramers. **E**. Representative flow cytometry of live CD19$^+$ CD3$^-$ CD14$^-$ CD16$^-$ B cells binding T-Ag PE tetramers but not GST PE650 control tetramers in blood samples from MCC patients and controls with and without enrichment with anti-PE microbeads prior to analysis. The displayed plots contain pooled cells from three individuals with or without MCC. **F, G**. Antibodies from ten T-Ag tetramer-binding human B cells were cloned and assessed for binding to T-Ag using Bio-Layer Interferometry (BLI). Five tested antibodies derived from patient samples and five from controls. Area under the curve (AUC) of the BLI shift for each antibody. Representative of two similar experiments.

Frequency of antigen-experienced B cells in the blood of female patients near the time of diagnosis associates with MCC progression.

After confirming that tetramer-binding B cells were T-Ag-specific, we analyzed blood cells from a prospective cohort of 47 T-Ag-driven MCC patients collected within 67 days of diagnosis and shortly before or after treatment initiation (**Figure S1**, **Table S2**). This cohort included 23 patients that experienced MCC progression within three years following our analysis, and 24 stage- and age-matched patients with non-progressive disease. In agreement with published data from larger

156 cohorts[12,13], the level of T-Ag-specific antibodies in blood prior to treatment was not associated with
157 MCC progression after treatment (**Figure S2c**). Also agreeing with published data[12,13], the level of T-
158 Ag-specific antibodies in blood diminished in most patients that did not experience MCC progression
159 whereas patients experiencing progressive MCC exhibited sustained or rising titers (**Figure S2d**).
160 Combined, the alignment of blood antibody data with previous work indicates the suitability of this
161 prospective MCC patient cohort for B cell analysis.
162 T-Ag-specific B cells represented ~0.09% of B cells in blood from MCC patients, which was
163 increased ~10-fold compared to control samples from individuals with no history of MCC (**Figure S2e**).
164 While the frequency of T-Ag-specific B cells ranged from 0.04 - 0.16% from patient-to-patient, there
165 was no association with the frequency of T-Ag-specific B cells and MCC progression (**Figure S2e**).
166 There was also no association between the frequency of T-antigen-specific B cells with the total level of
167 T-Ag-specific antibodies in the blood (**Figure S3**).
168 We next considered whether different B cell subtypes associated with disease outcome and
169 stratified the cohorts by sex because B cell phenotypes are affected by estrogen levels[31]. We first
170 assessed total antibody-secreting cells, which varied from 0.1 – 19% of B cells in blood and frequencies
171 did not associate with outcome (**Figures S2f, S4a**). T-Ag-specific antibody-secreting cells in blood were
172 usually below the limit of detection, and frequencies did not associate with outcome (**Figure S4b**). In
173 contrast, isotype-switched cells ranged from 3 - 54% of B cells and higher frequencies associated with
174 MCC progression in female patients, but not in male patients (**Fig S2f, g**). These associations were
175 maintained across several isotype-switched cell subtypes including $CD27^+$ memory B cells and $CD11c^+$
176 memory B cells (**Figure S2g**). The % of B cells that were isotype-switched and expressed CD71, which
177 indicates recent activation[21], was increased in both male and female MCC patients but did not
178 significantly associate with progression (**Figure S2g**). Intriguingly, the frequency of T-Ag-specific B cells
179 within each of these B cell subtypes was low and did not associate with MCC outcome, even when
180 stratified by sex (**Figure S2h, S4b**). Together, our results demonstrate that while the level of T-Ag-
181 specific antibodies or T-Ag-specific B cells did not associate with MCC outcome, higher frequencies of
182 total circulating isotype-switched B cells prior to treatment associated with worse outcomes in female
183 patients following MCC treatment.
184
185 *T-Ag-specific B cells are present in MCC tumors.*
186 The association between isotype-switched B cells in the blood with MCC progression for some
187 patients led us to consider whether stronger associations would be identified studying B cells from
188 tumor samples. For this we assessed a cohort of 19 patients with T-Ag-driven MCC from which single
189 cell tumor digests were cryopreserved (**Figure 2a**). Detailed patient histories were accounted for to
190 identify adverse clinical risk factors at the time of tumor removal that may confound survival analyses
191 (**Figure S5**, **Table S3**). Notably, 16 of the 19 tumor samples came from male patients, limiting
192 stratification by sex. Using known recurrence risk factors[32], eleven patients from this cohort were
193 considered to have low or medium risk for MCC progression, whereas eight patients were considered
194 high risk. These risk categories we unable to predict outcome within this cohort (**Figure 2b**). As
195 expected, T-Ag-specific antibodies at time of surgery also did not predict outcomes and were sustained
196 or increased in patients with progressive MCC (**Figure 2c, d**). Together, these results highlight the
197 need for additional biomarkers for more accurate MCC outcome prediction.
198 To study T-Ag-specific B cell responses in MCC tumors, we performed paired Cellular Indexing of
199 Transcriptomics and Epitopes by Sequencing (CITEseq) (**Tables S4, 5**) and antibody *IgH* + *IgL*
200 sequencing on five MCC skin tumor samples and fourteen MCC lymph node (LN) tumor samples.
201 Importantly, the presence of MCC in the LN samples was first detected during biopsy and later
202 confirmed during single cell sorting based on the increased presence of $CD56^+$ cells (**Figure 2e, f**).
203 From these tumor samples we FACS-purified $CD3^+$ T cells, $CD56^+$ MCC cells, and $CD19^+$ B cells that
204 bound T-Ag-tetramers or Respiratory Syncytial Virus (RSV) F antigen-tetramers but not control
205 tetramers, and B cells of unknown specificity that did not bind tetramers (**Figure 2e**). Expectedly,
206 frequencies of $CD19^+$ B cells were lower in MCC skin tumor samples when compared to blood or LN

tumor samples (**Figure 2f**). In contrast, the frequency of CD3+ T cells and CD56+ MCC cells were similar across both tumor sample types (**Figure 2f**). While the frequencies of B cells, T cells, and MCC cells varied greatly from sample-to-sample, associations with MCC progression were not detected (**Figure S6a**).

After standard processing and quality control metrics, we used uniform manifold approximation and projection (UMAP)[33] of single cell transcriptomic data from 1,015 immune-associated genes (**Table S4**), which identified clusters of MCC cells, T cells, and B cells (**Figures 2g, S7**). Within the B cell population, we identified cells that bound T-Ag tetramer-oligo but not RSV F or GST control tetramers (**Figure 2h**). We validated the specificity of our approach by confirming T-Ag binding of 87% (12/14) of antibodies derived from T-Ag tetramer-oligo+ B cells by BLI whereas none of the 10 antibodies cloned from tetramer− B cells bound T-Ag (**Figure 2i, j, Table S6**). Together, we analyzed 941 T-Ag-specific B cells, 36,641 B cells of unknown specificity, 58,708 CD3+ T cells, and 33,573 CD56+ MCC cells from MCC tumor samples. Within the cohort, 0.01 - 4% of B cells were T-Ag-specific in the 16 of 19 samples where these cells were detected (**Figure 2k**). Despite this high variability, no association between the frequency of T-Ag-specific CD19+ B cells and disease progression was detected (**Figure S6b**).

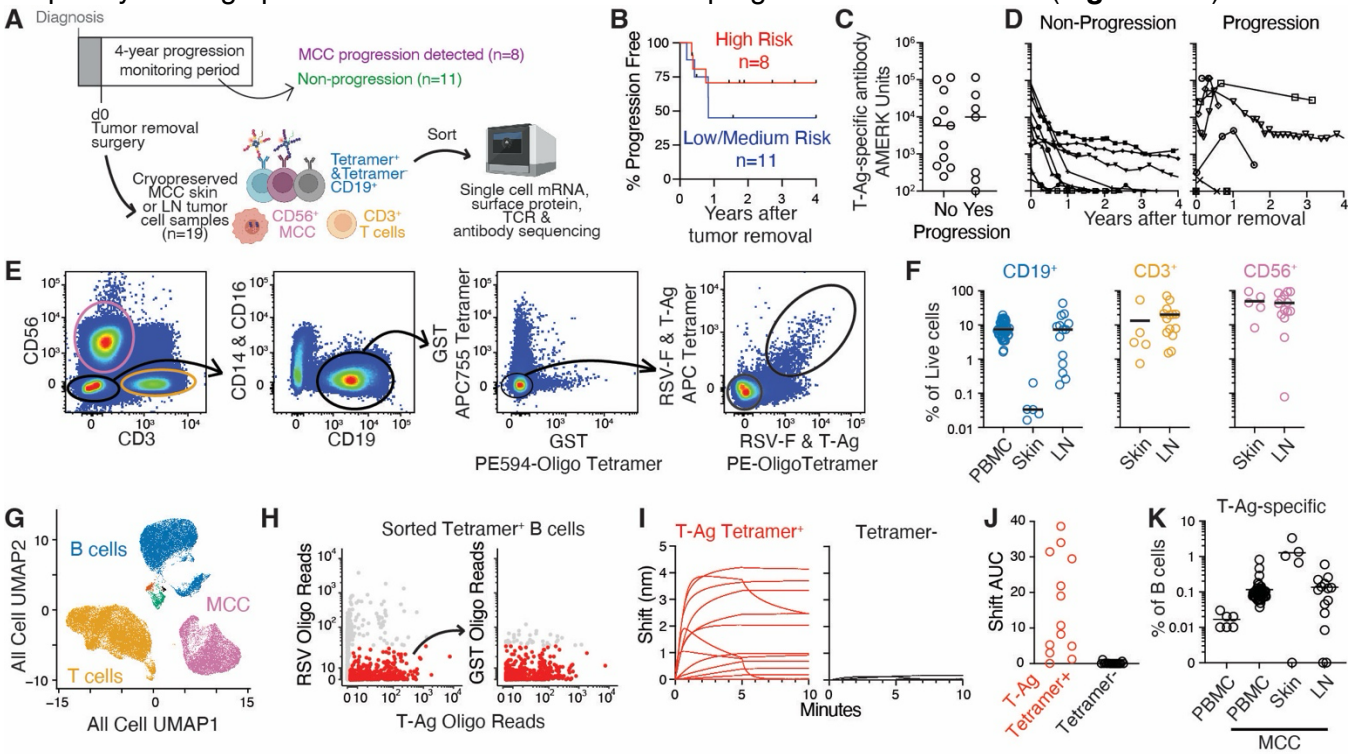

Figure 2. Identification and analysis of T-Ag-specific B cells from T-Ag-driven MCC patient tumor samples. **A**. Schematic representation of single cell RNA-sequencing experiments assessing B cells, T cells and MCC cells from skin tumor and LN tumor samples. **B**. Kaplan-Meier plots displaying percent progression-free survival for patients during the four-year monitoring period following tumor removal surgery stratified based on clinical risk scoring of data available at the time of surgery. **C**. Level of T-Ag-specific antibodies in the blood of MCC tumor cohort patients near the time of diagnosis stratified based upon whether patients experienced MCC progression (n=8) or not (n=11) during the four-year monitoring period. **D**. Longitudinal analysis of T-Ag-specific antibodies in the blood of MCC tumor cohort patients. Two patients from the non-progressive group for which antibody levels were not available for at least a year after diagnosis were excluded. **E**. Representative flow cytometry of CD3+ T cells, CD56+ MCC cells, and CD19+ B cells that bound pooled T-Ag and RSV F APC and PE-oligo tetramers but not APC755 and PE594-oligo control tetramers and B cells of unknown specificity that did not bind any tetramers. **F**. Pooled data from seven experiments showing the % of CD19+ B cells, % of CD3+ T cells, and % of CD56+ MCC cells in skin tumor (n=5), and LN tumor (n=14) samples from MCC patients determined by flow cytometry. **G**. UMAP clustering of CITEseq data of cells pooled from all skin and LN tumor samples after alignment and normalization with highlighted clusters of T cells (yellow), B cells (blue), MCC cells (pink), and contaminating cells (red, green). **H**. Computational strategy to identify T-antigen tetramer-binding B cells. **I, J**. Antibodies from thirteen

T-Ag tetramer-binding B cells and ten from control B cells were cloned and assessed for binding to T-Ag using BLI. Representative of two similar experiments. **K**. Pooled data from seven experiments displaying the % of CD19+ B cells specific for T-Ag in MCC skin and LN tumor samples compared to the frequency found in blood.

T-Ag-specific antibody-secreting cells in MCC tumor samples associates with MCC control.

To assess B cell subtypes in patient tumor samples, B cells were subclustered and populations corresponding to antibody-secreting cells, germinal center B cells, memory B cells, and naïve B cells were identified (**Figure 3a, b**). B cells that did not cluster with these canonical subsets were also present and did not appear to be activated B cells since CD71 expression was not detected (**Figure 3a, b**). All analyzed B cell subtypes were observed in T-Ag-specific B cells and the much more numerous B cells of unknown specificity, with highly varied frequency distributions across the cohort (**Figure 3c**). Notably, two LN tumor samples contained a concurrent B cell malignancy (**Figure 3a, b**), Mantle Cell Lymphoma (MCL) or Chronic Lymphocytic Leukemia (CLL). For these, MCL and CLL cells were excluded to focus only on non-malignant B cells for subtype analyses.

Since increased frequencies of isotype-switched B cells in the blood associated with MCC progression for some patients, we next assessed memory B cells in tumor samples as a population able to exit the tissue and enter the blood. Memory B cells were detected in every tumor sample and ranged from 6 - 82% of B cells (**Figure 3d**). T-Ag-specific memory B cells exhibited similar variability but were not detected in three LN tumor samples and one skin tumor sample (**Figure 3d**). In LN tumor samples, the frequency of T-Ag-specific memory B cells correlated with the total frequency of memory B cells (**Figure 3e**). Higher frequency of T-Ag-specific or total memory B cells in tumor samples did not associate with MCC progression (**Figure 3f**). Since MCC skin lesion samples were limited, these analyses were conducted with LN tumor samples alone or combined with skin tumor samples (**Figure 3f**). Intriguingly, lower frequency of T-Ag-specific memory B cells in LN tumor samples trended towards an association with MCC progression but did not achieve statistical significance (**Figure 3f**).

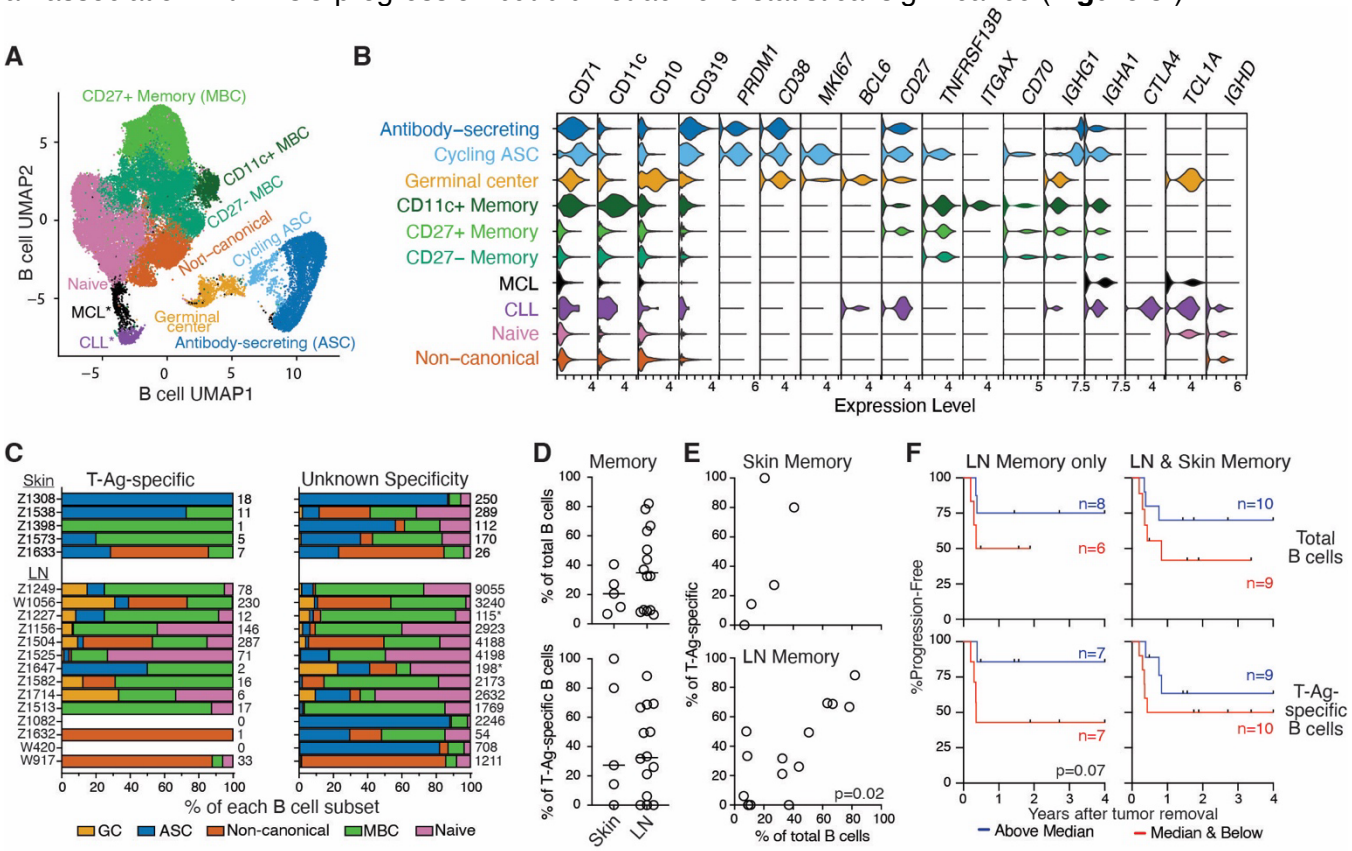

Figure 3. Phenotypes of T-Ag-specific B cells in MCC tumors. A. UMAP clustering of single cell RNA expression by B cells from pooled skin (n=5) and LN (n=14) tumor samples with clusters corresponding to different B cell subtypes highlighted with different colors. **B**. Violin plots showing expression of select genes

268 used to identify B cell subtypes. **C**. Stacked bar graphs displaying the % of T-Ag-specific and B cells of
269 unknown specificity of each subtype found in individual patients. The numbers to the right of each stacked bar
270 indicate the number of cells assessed in that stacked bar. *Indicates samples in which CLL or MCL cells were
271 excluded from subset analysis. **D**. % of total (top) and T-Ag-specific (bottom) B cells that were memory in skin
272 and LN tumor samples. The bars indicate median for each tissue type. **E**. % of T-Ag-specific B cells that were
273 memory versus % of total B cells that were memory in each skin (top) and lymph node (bottom) tumor samples.
274 Correlation p value was determined using nonparametric Spearman's test. **F**. Kaplan-Meier plots displaying %
275 progression-free survival for patients during the monitoring period following analysis divided into groups with
276 a % of total (top) and T-Ag-specific (bottom) B cells that were memory above (blue) or at/below (red) the
277 median. The p value nearing significance generated using Mantel-Cox Log-rank test.
278
279 Antibody-secreting cells also exhibited high sample-to-sample variability, accounting for 10 - 87%
280 and 1 - 85% of $CD19^+$ cells in skin and LN tumor samples, respectively (**Figure 4a**). Variability was
281 similar within the T-Ag-specific B cell population, except that T-Ag-specific antibody-secreting cells
282 were not detected in one skin tumor sample and half of the fourteen LN tumor samples (**Figure 4a**).
283 Unlike memory B cells (**Figure 3e**), higher frequency of T-Ag-specific antibody-secreting cells did not
284 correlate with frequencies of total antibody-secreting cells in MCC tumor samples (**Figure 4b**).
285 Similarly, the frequency of T-Ag-specific antibody-secreting cells in MCC tumor samples did not
286 correlate with levels of T-Ag-specific antibodies in the blood at the time of tumor removal (**Figure 4c**).
287 The lack of correlation between levels of antibody in blood and frequency of detected antibody-
288 secreting cells did not appear to be the result of IgG being detected in blood and antibody-secreting
289 cells of all isotypes being interrogated since nearly all antibody-secreting cells detected were IgG^+
290 (**Figure 4d**). Combined, these data suggested that the antibody-secreting cell response detected in
291 tumor samples is distinct from what can be inferred from analysis of serum antibodies in the blood.
292 We next considered whether antibody-secreting cell frequencies in tumor samples associated with
293 MCC outcome after treatment. Since MCC skin lesion samples were limited, we conducted separate
294 analyses either with LN tumor samples alone or combined with skin tumor samples. Strikingly, we
295 found the presence of detectable T-Ag-specific antibody-secreting cells in LN tumor samples was
296 associated with extended progression-free survival following tumor removal (**Figure 4e**). Similar results
297 were found when skin tumor samples were included based upon whether the frequency of T-Ag-
298 specific antibody-secreting cells was above or below the median found in skin tumors (**Figure 4e**). In
299 contrast, a higher frequency of total antibody-secreting cells in skin or LN tumors was not associated
300 with MCC outcome (**Figure 4e**). To further probe relationships between antibody-secreting cells and
301 MCC progression, we used multiplex immunohistochemistry (mIHC) to assess an independent cohort
302 of 23 MCC LN tumor and 63 MCC skin tumor sections (**Figure 4f, S8**, **S9, Table S7**). As observed by
303 CITEseq, the frequency of $CD138^+$ antibody-secreting cells within $CD19^+$ cells in MCC tumors varied
304 widely but did not differ between regions of tumor mass and adjacent non-tumor tissue stroma (**Figure**
305 **4f, g**). Similarly, the frequency of antibody-secreting cells out of total B cells tumor mass or adjacent
306 non-tumor tissue stroma did not associate with MCC outcomes for skin or LN tumor samples (**Figure**
307 **4h**). Together, our results indicate that while high frequencies of antibody-secreting cells in MCC tumor
308 samples does not associate with MCC outcome, the absence of detectable T-Ag-specific cells within
309 this population associates with MCC progression.

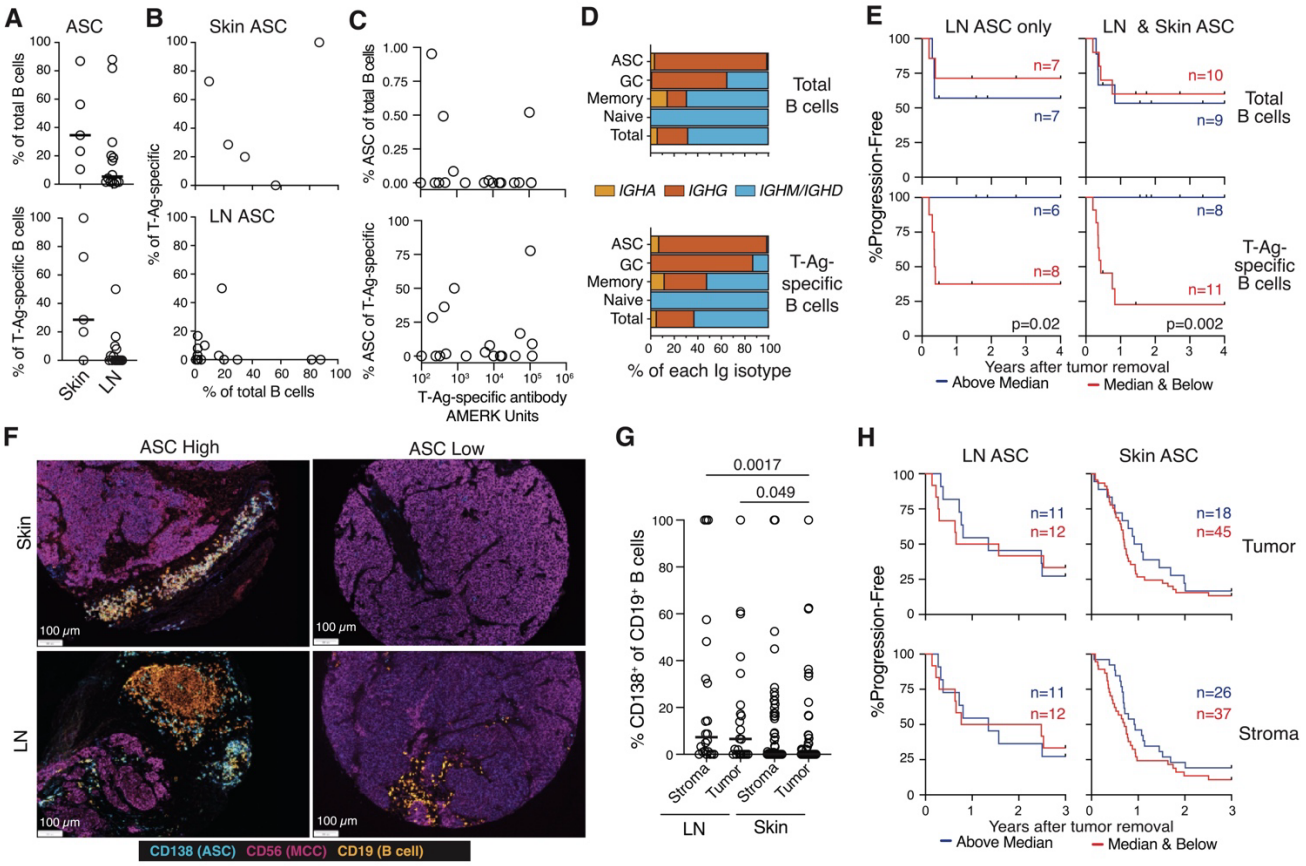

Figure 4. Lower frequency of T-Ag-specific antibody-secreting cells in MCC tumors associates with progressive disease.

A. Data from single cell sequencing experiments showing the % of total (top) and T-Ag-specific (bottom) antibody-secreting cells in skin and LN tumor samples. Bars indicate medians. **B**. % of T-Ag-specific cells that were antibody-secreting versus the % of all B cells that were antibody-secreting in skin (top) and LN (bottom) tumor samples. **C**. Level of T-Ag-specific antibodies in the blood of MCC patients near the time of surgery versus the % of T-Ag-specific or total B cells that were antibody-secreting in skin tumor (top) and LN (bottom) tumor samples. **D**. % of B cells of total (top) or T-Ag-specific B cells of the listed B cell subtype that expressed *IGHM/IGHD* or class-switched to *IGHA* or an *IGHG.* **E**. Kaplan-Meier plots displaying % progression-free survival for patients during the monitoring period divided into groups with a % of total (top) and T-Ag-specific (bottom) B cells that were antibody-secreting above (blue) or at/below (red) the median. Significant p values generated using Mantel-Cox Log-rank test are displayed. **F**. Select mIHC images of skin and lymph node tumor samples determined to contain high or low frequencies of CD19+ CD138+ antibody-secreting cells. **G**. % of CD19+ cells that were CD138+ antibody-secreting cells within the CD56+ tumor tissue or adjacent non-tumor stroma detected using mIHC of LN (n=23) and skin tumor samples (n=63). **H**. Kaplan-Meier plots displaying % progression-free survival for patients during a three-year monitoring period following analysis stratified based on % of B cells that were antibody-secreting above (blue) or at/below (red) the median within the tumor tissue (top) and adjacent non-tumor stroma (bottom) determined by mIHC.

Germinal center response in MCC tumor samples associates with MCC control.

The presence of tertiary lymphoid structures able to support germinal centers in tumors associates with better outcomes for many solid cancers[17-19]. We identified T-Ag-specific germinal center B cells in eight of the fourteen LN tumor samples but failed to detect any in skin tumor samples (**Figure 5a**). Few germinal center B cells were detected in skin tumor samples overall (**Figure 5a**) in agreement with previous work demonstrating limited development of organized tertiary lymphoid structures in MCC skin tumor samples[34-36]. Among the LN tumor samples, higher frequencies of T-Ag-specific germinal center B cells trended with higher frequencies of total germinal center B cells (**Figure 5b**) even though T-Ag-specific cells made up less than 1% of germinal center B cells when detected (**Figure 5c**). Remarkably,

339 the presence of detected T-Ag-specific germinal center B cells in LN tumor samples was predictive of
340 prolonged progression-free survival, whereas absence of these cells associated with rapid disease-
341 progression (**Figure 5d**). Interestingly, higher frequencies of total germinal center B cells in LN tumor
342 samples also associated with progression-free survival (**Figure 5d**).
343 Because robust germinal center B cell responses are dependent on signals from follicular helper
344 CD4+ T cells (T_{FH}), we assessed whether this T cell population associated with MCC outcome. Sub-
345 clustering of CD4+ T cells revealed a population of cells with a T_{FH} signature[37] that included increased
346 expression of *BCL6*, *PDCD1*, *CXCL13*, and *TCF7* transcripts (**Figure 5e, f**). CD4+ T cells in this cluster
347 were detected in both skin and LN tumor samples but were more abundant in LN (**Figure 5g**). Like the
348 germinal center B cell response, frequencies of T_{FH} cells above the median in LN tumor samples were
349 also predictive of progression-free survival, whereas patients whose tumors had less T_{FH} cells were
350 more likely to have rapid MCC progression (**Figure 5h**). Expectedly, tumor samples with more T_{FH} cells
351 tended to have higher frequencies of T-Ag-specific and total germinal center B cells (**Figure 5i**). In
352 contrast, none of the five other CD4+ T cell clusters associated with disease outcome (**Figure 5g, h**).

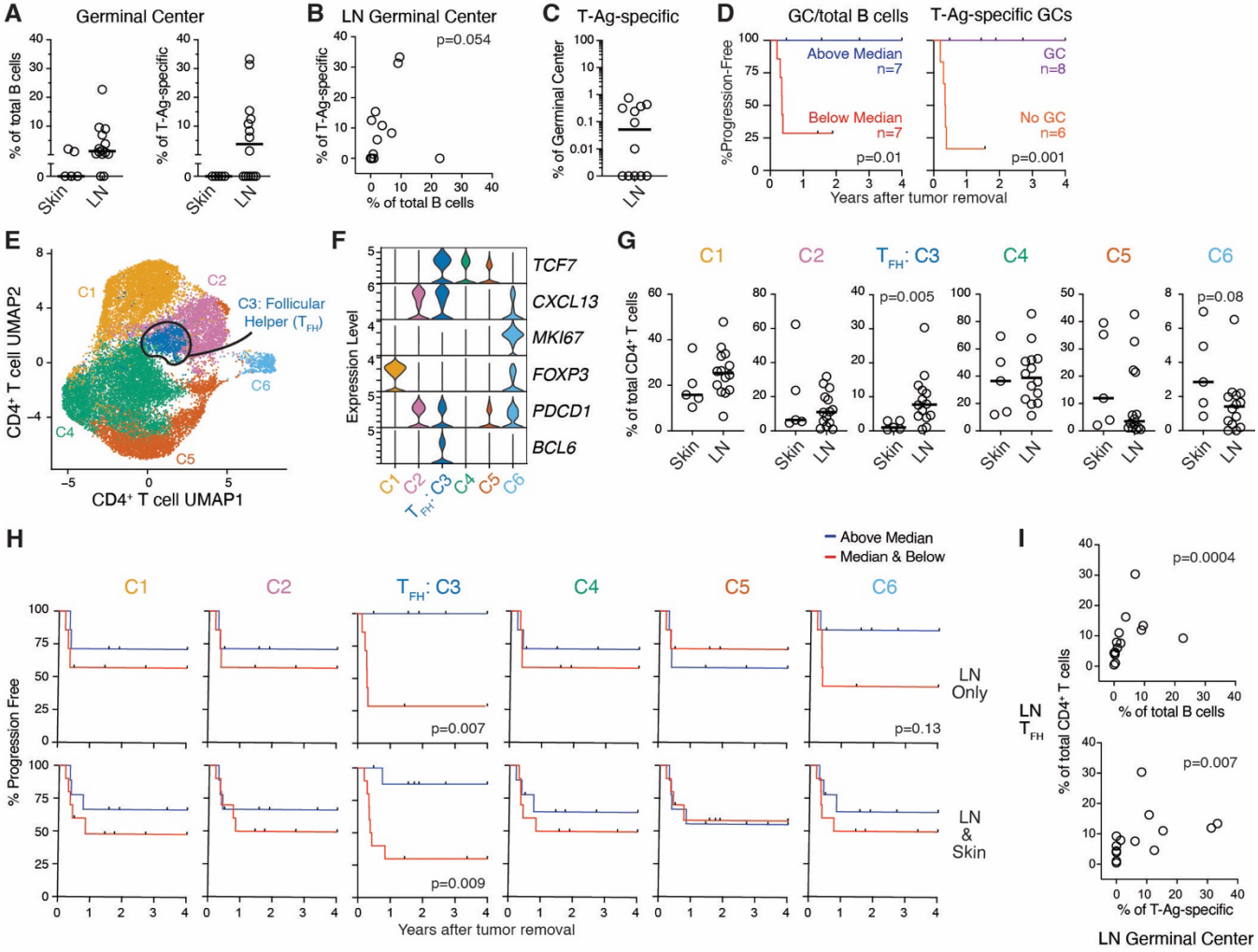

353
354 **Figure 5: Lower frequency of germinal center B cells and T_{FH} cells in MCC tumor samples associates with**
355 **progressive disease.**
356 **A**. Data from single cell sequencing experiments showing the % of total (top) and T-Ag-specific (bottom) B cells
357 that were germinal center phenotype in skin and LN tumor samples. Bars indicate medians. **B**. % of T-Ag-specific
358 B cells that were germinal center phenotype versus the % of all B cells that were germinal center phenotype in
359 LN tumor samples. Correlation p value determined using nonparametric Spearman's test. **C**. % of T-Ag-specific
360 cells within the total germinal center B cell population in LN tumor samples. **D**. Kaplan-Meier plots displaying %
361 progression-free survival for patients during the four-year monitoring period following analysis divided into groups
362 with a % of total B cells (left) that were germinal center phenotype above (blue) or at/below (red) the median and

363 whether T-Ag-specific (right) germinal center phenotype cells were detected (violet) or below the limit of detection
364 (orange). Displayed p values generated using Mantel-Cox Log-rank test. **E**. UMAP clustering of single cell RNA
365 expression by $CD4^+$ T cells from pooled skin (n=5) and LN (n=14) tumor samples with clusters corresponding to
366 subtypes highlighted with different colors. **F**. Violin plots showing the expression of select genes used to identify
367 T_{FH} cells. **G**. % of $CD4^+$ T cells that were in each cluster within skin and LN tumor samples. Bars indicate median
368 and significant p value generated using a non-parametric Mann-Whitney test is displayed. **H**. Kaplan-Meier plots
369 displaying % progression-free survival for patients during the four-year monitoring period following analysis
370 divided into groups with a % of $CD4^+$ T cells that were in each cluster above (blue) or at/below (red) the median.
371 Significant p values generated using Mantel-Cox Log-rank test are displayed. **I**. % of total (left) and T-Ag-specific
372 (right) B cells that were germinal center phenotype versus the % of CD4+ T cells that were T_{FH} in LN tumor
373 samples. Correlation p values determined using nonparametric Spearman's test.
374
375 *T-Ag-specific B cells potently activate T-Ag-specific $CD4^+$ T cells.*
376 To confirm the presence of T-Ag-specific T_{FH} cells in MCC tumors, we examined paired TCRα/β
377 CDR3 sequences from $CD4^+$ T cells from three patient tumors. This analysis revealed that 31%
378 (408/1315) of these cells shared identical paired TCRα/β CDR3 sequences with at least one other cell,
379 indicating clonal expansion (**Figure 6a, Table S8**). TCRs from 69 clonal families containing *CXCL13*$^+$
380 members were expressed in primary $CD4^+$ T cells derived from healthy donors using a previous
381 described lentiviral transduction approach[37] (**Figure 6b**). Transduced T cells were next assessed for T-
382 Ag specificity by incubation with autologous B cells in the presence and absence of T-Ag peptides. This
383 assay revealed that 23% (16/69) of tested clonal TCRs secreted IFNγ in response to pools of T-Ag
384 peptides (**Figure 6c, S10, Table S9**), confirming specificity for T-Ag.
385 We next considered whether T-Ag-specific B cells could more potently stimulate T-Ag-specific $CD4^+$
386 T cells compared to B cells of unknown specificity. For this, we cultured lentiviral-transduced T-Ag-
387 specific $CD4^+$ T cells with CRISPR-engineered T-Ag-specific B cells generated using a previously
388 described approach[38]. For these assays we used a cocktail of constructs encoding the three T-Ag-
389 specific antibodies, 1G04, 2H04, and 1B09 (**Figure S1F**) to simulate an oligoclonal B cell population.
390 Antibody constructs containing DNA producing the full antibody light chain physically linked to the
391 heavy chain VDJ with a 57 amino acid glycine-serine linker[39] were pooled prior to engineering was
392 expression was validated based upon binding T-Ag tetramer and Strep-Tactin (**Figure 6d**), which binds
393 Strep-tagII[40-42] included in the linker. These assays revealed that T-Ag-specific engineered B cells from
394 a healthy donor that expressed the HLA DR4-DQ8 haplotype that presents the T-Ag could induce
395 similar levels of CD69 and OX40 by $CD4^+$ T cells expressing the T-Ag-specific TCR F5 in response to
396 100-fold lower concentrations of purified T-Ag compared to control B cells (**Figure 6e, f**). T-Ag-specific
397 engineered B cells could also stimulate CD69 and OX40 by T-Ag-specific F5 TCR $CD4^+$ T cells in
398 response to MCC cell lysate from a tumor cell line, which was not found with control B cells (**Figure
399 6g**). Combined, these data indicate that T-Ag-specific B cells can potently activate T-Ag-specific $CD4^+$
400 T cells.

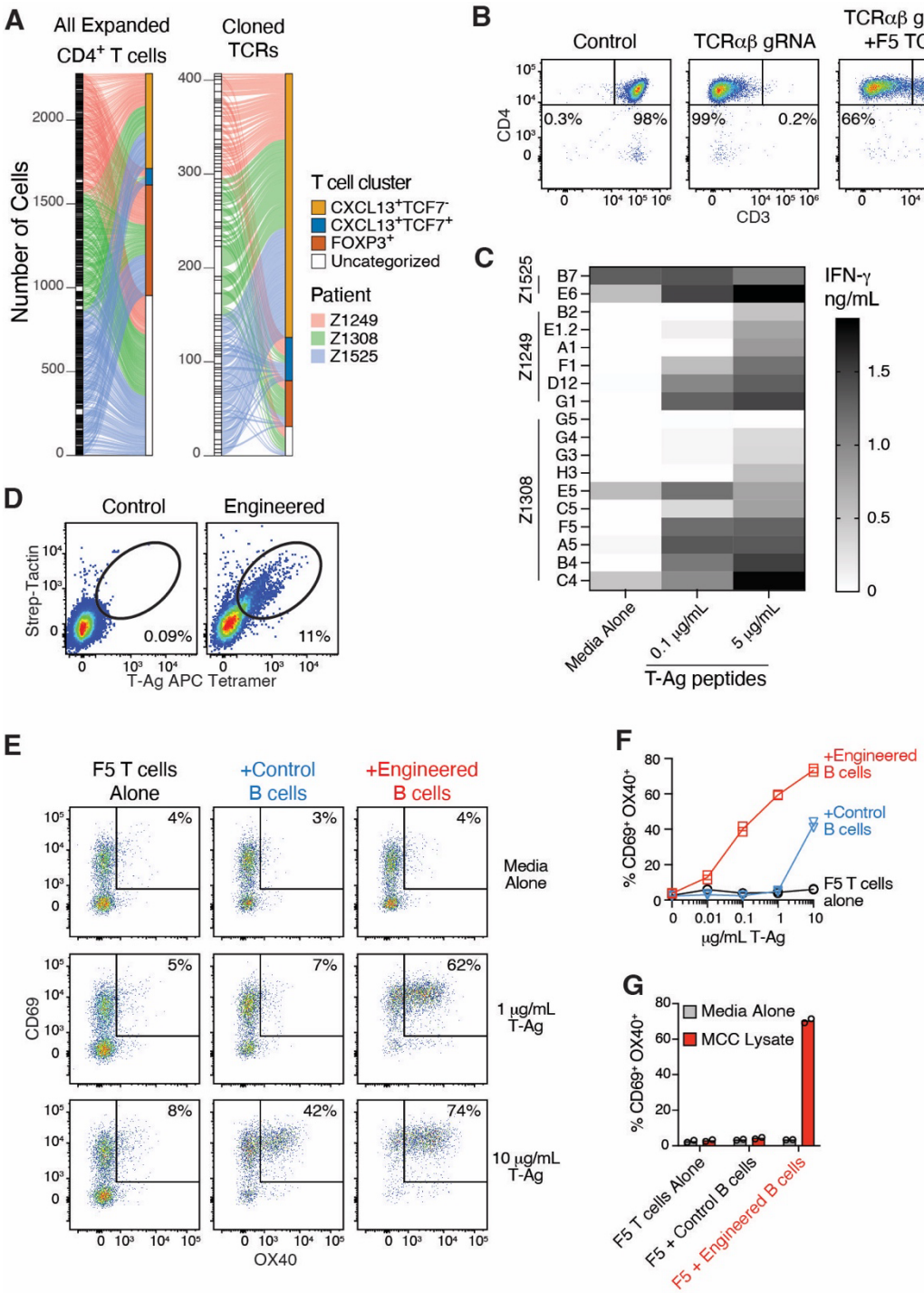

Figure 6. T-Ag-specific engineered B cells potently stimulate T-Ag-specific engineered CD4+ T cells.

A. TCRs expressed by all CD4+ T cells (left) and identical TCRs expressed by multiple cells (right) from three LN and skin tumor samples linked to cell subtype. **B**. Representative flow cytometry of the expression of lentiviral-expressed T-Ag-specific TCR in CD4+ from blood detected as the expression of CD3 on the cell surface in cells lacking endogenous TCR due to CRISPR knockout using gRNA targeting TCRα and TCRβ. **C**. Eighteen clonal T_{FH} TCRs from MCC tumor samples were expressed via lentivirus in CD4+ cells from blood and incubated with sample-matched B cells in the absence or presence of 0.1 or 5 μg/mL of T-Ag peptide pools for three days prior to assessment of supernatant for secreted IFNγ. Representative of two similar experiments. **D**. Representative flow cytometry of Strep-Tactin

and T-Ag binding to human B cells engineered to express a T-Ag-specific antibodies using CRISPR/Cas9. Antibody constructs encoding 1G04, 2H04, and 1B09 from containing the full antibody light chains physically linked to the heavy chain VDJs with a linker[39] containing Strep-tagII[40-42] were pooled prior to engineering. **E**. Representative flow cytometry and (**F**) quantitation of CD69 and OX40 expression by lentiviral-transduced T-Ag-specific F5 TCR $CD4^+$ T cells expressing following 72-hour co-culture with CRISPR-engineered T-Ag-specific oligoclonal B cells or control B cells in the presence or absence of various concentrations of T-Ag. **G**. Quantitation of CD69 and OX40 expression by lentiviral-transduced T-Ag-specific F5 TCR $CD4^+$ T cells expressing the were co-cultured for 24 hours with CRISPR-engineered T-Ag-specific oligoclonal B cells or control B cells in the presence or absence of MCC cell line lysate. **E**-**G** representative of two similar experiments.

Antibody-secreting cells and memory B cells in tumor samples are largely germinal center-derived.

Our data demonstrated that the T-Ag-specific germinal center and antibody-secreting B cell responses in MCC tumors associate with better progression-free survival (**Figure 4e, 5d**). Since antibody-secreting cell differentiation can occur through germinal-center dependent and independent pathways, we analyzed paired antibody heavy and light chain sequences and clonal dynamics of B cells in MCC tumor samples for evidence of somatic hypermutation in a germinal center.

To assess somatic hypermutation in B cells from MCC tumors, we determined the mutation frequency in *IgH* sequences with respect to germline encoded sequences. Most T-Ag-specific antibody-secreting cells and germinal center B cells had *IgH* mutations at similar levels to B cells of unknown specificity with these phenotypes (**Figure 7a**). Somatic hypermutation was also present in T-Ag-specific memory B cells found in tumor samples, even in samples where germinal center B cells were not detected (**Figure 7a**). Similarly, *IgH* mutation frequencies were similar in B cells from skin and LN tumor samples, independently of T-Ag specificity (**Figure 7b**). Notably, the frequency of somatic hypermutation did not associate with MCC progression (**Figure 7c**).

While somatic hypermutation strongly suggested that T-Ag-specific antibody-secreting cells and memory B cells derived from germinal centers, we sought to confirm this by analysis of clonal families containing germinal center and non-germinal center members. Analysis of paired *IgH* + *IgL* sequences revealed that B cells from skin tumor samples were slightly more clonally related than B cells from LN tumor samples (**Figure 7d**). In total, we identified 4,119 expanded B cells of unknown specificity amongst 589 clonal families spread across 17 MCC patient tumor samples (**Figure 7e**). T-Ag-specific B cell clonal families were only found in 7 of the 19 tumor samples and amounted to 150 expanded cells amongst 42 clonal families (**Figure 7f, Table S10**). Intriguingly, six of the seven samples with detectable clonal families were from patients who did not progress, with the smallest clonal family being derived from lymph node tumor sample from patient Z1513, who experienced MCC progression (**Figure 7f, S5**).

Not surprisingly, the three LN tumor samples with the most abundant T-Ag-specific B cell clonal families contained mutated antibody-secreting cells and germinal center B cells within the same clonal family (**Figure 7f**). In fact, 10 of the 18 T-antigen-specific clonal families containing an antibody-secreting B cell also contained a germinal center B cell (**Figure 7f**). These results demonstrated that T-Ag-specific antibody-secreting cells and memory B cells can derive from germinal centers found in LN tumor samples.

As a final analysis we compiled the analyses of B cells and T cells to determine if combinations of parameters better predicted disease outcome (**Figure 7g**). When assessed together, we found that tumor samples from all eight MCC patients in the cohort that that later experienced MCC progression contained low frequencies of T-Ag-specific germinal center B cells, low frequencies of T-Ag-specific antibody-secreting cells, undetectable T-Ag-specific B cell clonal families, low frequencies of total germinal center B cells, and low frequencies of T_{FH} cells (**Figure 7g, h**). In contrast, all eleven MCC patients had higher frequencies of at least two of these five B cell and T cell readouts (**Figure 7g, h**).

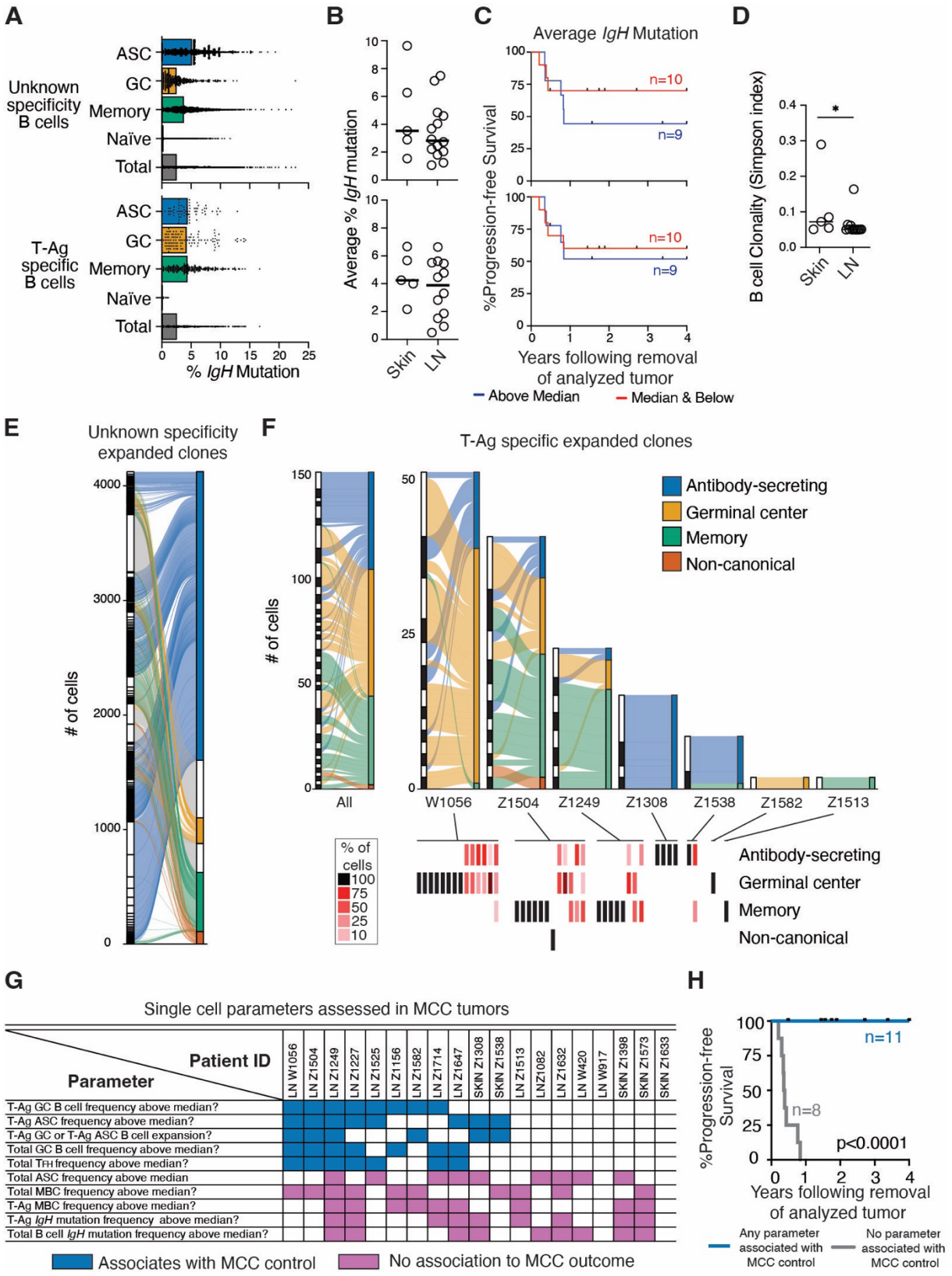

Figure 7: Analysis of somatic hypermutation and clonality indicates many antibody-secreting cells and memory B cells in tumors are germinal center-derived.

A. % of mutated *IgH* nucleotides for cells within the listed subpopulations of B cells of unknown specificities (top) and T-Ag-specific B cells (bottom). **B**. Average % of mutated *IgH* nucleotides for B cells of unknown specificities (top) and T-Ag-specific B cells (bottom) found in skin and LN tumor

samples. **C**. Kaplan-Meier plots displaying % progression-free survival for patients during the monitoring period following analysis divided into groups with a % mutation rate above (blue) or at/below (red) the median. **D**. Assessment of clonality within the B cells found in skin and LN tumor samples using Simpson Diversity Index. **E**. Stacked clonal lineage alluvial plot with lines linking individual cells within clonal families (left) with the B cell subtype (right) of that cell within B cells of unknown specificities. Each clonal family is displayed as an individual bar stacked in alternating black and white sized corresponding to the number of cells detected in that clonal family. **F**. Stacked clonal lineage plots (top) and heatmaps (bottom) of all T-Ag-specific clonal families from LN and skin tumor samples, and plots divided into individual patients. The columns in the heat maps correspond to individual clonal families. **G**. Summary of findings from analyses of B cells and T cells with phenotypes with significant associations with MCC control highlighted in blue. **H**. Kaplan-Meier plots displaying % progression-free survival for patients during the monitoring period following analysis divided into a group with any of the B or T cell characteristics associated with MCC control from **G** (blue), versus the group that did not have any of those characteristics. The p value generated using Mantel-Cox Log-rank test.

Discussion

Increasing evidence suggests an important role for B cells in immune control of tumors. Here we directly analyzed B cells specific for T-Ag oncoprotein during MCC in search of biomarkers able to predict MCC progression. Similar to analyses of T-Ag-specific antibodies in the blood[12,13], analysis of T-Ag-specific B cells in the blood near the time of diagnosis did not yield associations with disease progression. Intriguingly, increased frequencies of isotype-switched total B cells in the blood of female patients did associate with disease progression. It is intriguing to speculate that these links are related to the role estrogen plays in mediating increased levels of isotype-switched B cells in the blood[31].

We also found increasedisotype-switched CD71$^+$ B cells in the blood of both male and female MCC patients. This is not surprising given that CD71 is a marker of B cells recently activated by antigen in response to cancer and vaccination[21]. It is unclear what antigen these activated CD71$^+$ B cells are recognizing since the vast majority did not bind the portion of T-Ag usedhere. Some of these activated CD71$^+$ B cells could be specific for regions of large T-Ag that are not conserved from patient-to-patient. Alternatively, these activated CD71$^+$ B cells could be specific for self-antigens since self-antigen-specific antibodies are found in many cancers[43,44].

Findings from B cell populations in the blood were intriguing but not robust enough to be clinically actionable biomarkers, prompting assessment of B cells from 19 MCC patient tumor samples which revealed several predictive biomarkers of MCC progression. We found that ongoing germinal center B cell responses and high frequencies of T-Ag-specific antibody-secreting cells in tumor samples predicted control of MCC after treatment with remarkable accuracy. Given the strong predictive ability of T-Ag-specific B cell phenotypes in tumors, it was surprising that the level of T-Ag-specific antibodies in blood at the time of treatment is not predictive of outcome. We hypothesize that this difference is reflective of T-Ag-specific B cell responses we are unable to measure, such as responses in the weeks prior to tumor surgical excision, or responses in anatomical locations we are unable to assess, such as sites of disease spread or unaffected draining lymph nodes. This hypothesis is supported by our data indicating the presence of somatic hypermutation in most T-Ag-specific B cells in tumors even when germinal center responses are not detected.

Studies in other cancers analyzing the presence of antibody-secreting cells in tumors have often reported positive, negative, and no associations with disease outcome[45]. Our work studying the overall antibody-secreting cell responses using flow cytometry and immunofluorescence did not find an association with MCC progression. However, by studying T-Ag-specific B cells, we found a strong association between low frequencies of T-Ag-specific antibody-secreting cells and MCC progression. These data raise questions about the specificities and differentiation pathways of the more numerous antibody-secreting cells that are not T-Ag specific.

While we found several promising biomarkers of progressive MCC, more work is needed to understand the mechanism. Enhanced T-Ag-specific germinal center B cell and antibody-secreting cell responses in MCC tumor samples may reflect of an overall more robust immune response resulting in more tumor killing. In this scenario B cells are responding to the presence of more T-Ag released from

520 killed MCC cells. However, if more cell-free T-Ag is present, the levels of T-Ag-specific antibodies in
521 blood may also be expected to be increased, which is not the case. The association of T_{FH} cell
522 frequencies with MCC control, but not other $CD4^+$ T cell subsets, also suggests a role for B cells. If
523 increased B cell responses are merely of reflection of an overall better tumor-killing immune response,
524 a specific increase in T_{FH} cells would not be required as numerous $CD4^+$ populations would be
525 expected to be increased if merely a reflection of overall immune potency.
526 We hypothesize that T-Ag-specific B cells help enhance the response of T-Ag-specific T cell killing
527 of tumors. In support of this, we show that B cells engineered to be T-Ag-specific can potently activate
528 $CD4^+$ T cells expressing a T-Ag-specific TCR derived from a patient tumor sample. While it is unlikely
529 that $CD4^+$ T cells directly kill MCC due to the lack of MHC class II expression by MCC, $CD4^+$ T cells can
530 enhance antitumor $CD8^+$ T cell responses[20,46,47]. Likewise, data from a mouse model has suggested
531 that B cell stimulation of T_{FH} cells enhances IL-21 production which in turn enhances tumor killing by
532 $CD8^+$ T cells[20]. Newly generated mouse models of MCC[48] will likely help to answer these questions.

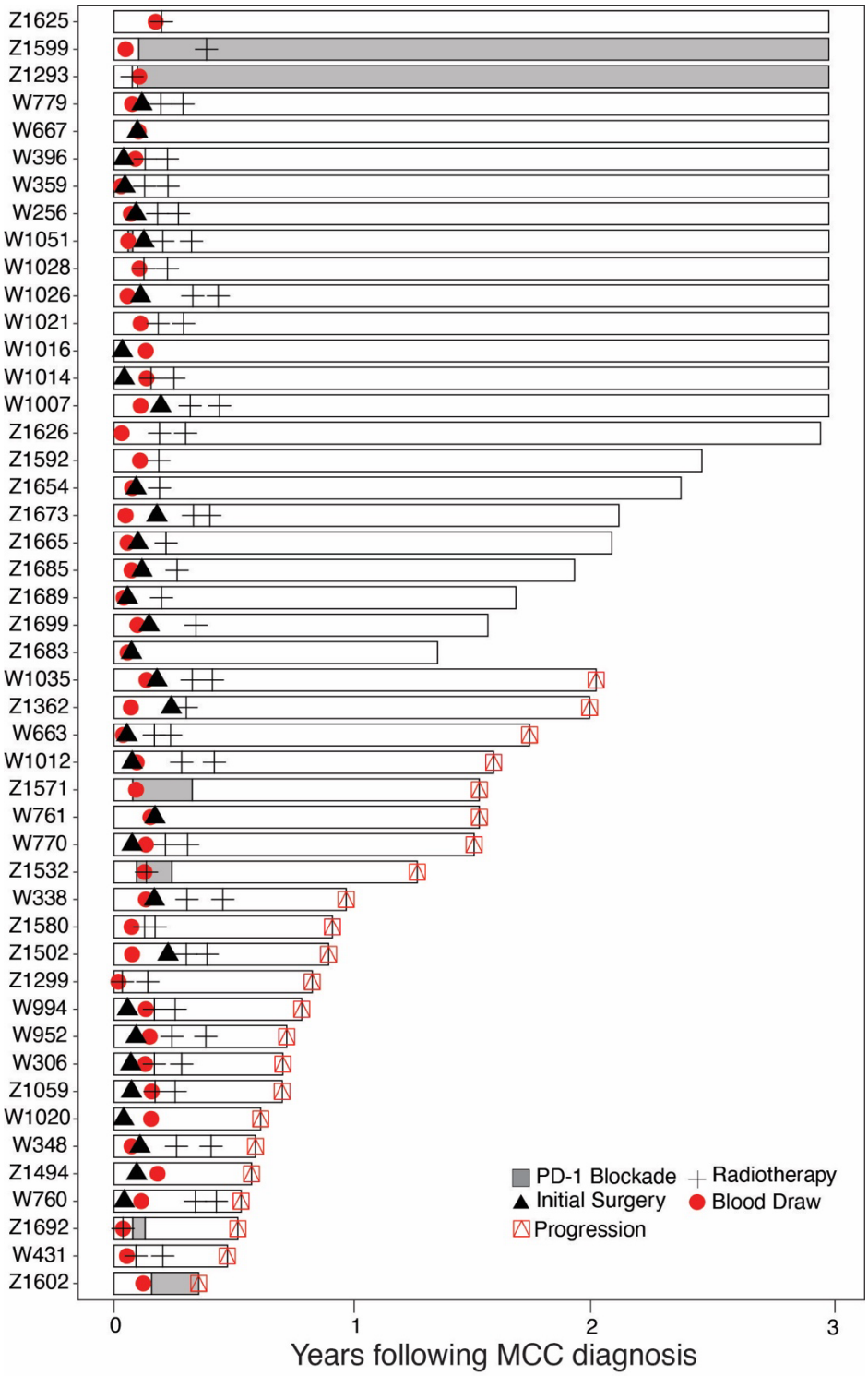

Supplemental Figure 1. PBMC cohort patient history summaries.

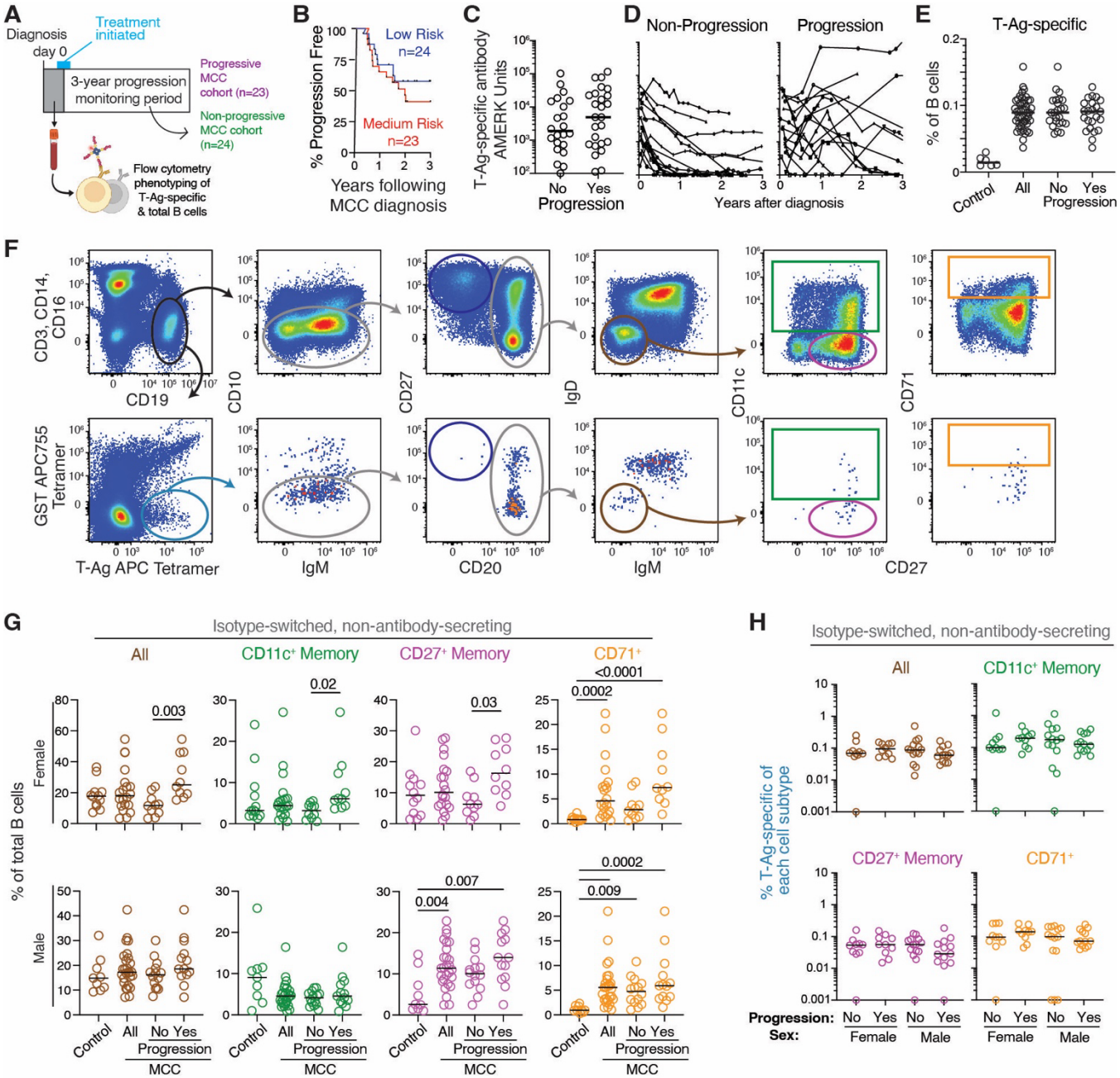

Supplemental Figure 2. Higher frequency of antigen-experienced B cells in blood of female patients near diagnosis associates with MCC progression.

A. Schematic representative of prospective cohorts used for experiments analyzing T-Ag-specific antibodies and B cells from MCC patient blood 6-67 days after MCC diagnosis. Patients were monitored for at least 3 years after treatment and stratified into a cohort that experienced progression (n=23) and a cohort that did not experience progression (n=24). **B**. Kaplan-Meier plots displaying percent progression-free survival for patients during the three-year monitoring period following treatment stratified based on clinical risk scoring of data available at the time of MCC diagnosis. **C**. Level of T-Ag-specific antibodies in the blood of MCC patients determined using AMERK near the time of diagnosis for the progression and non-progression cohorts. Bars represent medians. **D**. Longitudinal analysis of T-Ag-specific antibodies in the blood of MCC patients in the progression cohort (n=13) and non-progressive cohort (n=19). Patients for which antibody levels were not available for at least a year after diagnosis were excluded. **E**. Combined data from seven experiments showing the % of B cells binding T-Ag tetramers but not control tetramers in the blood of MCC patient cohorts. Bars represent

551 medians and significant p values determined by non-parametric Dunn's multiple comparison test are
552 displayed. **F**. Representative flow cytometry of CD27^{++} CD20^{-} CD10^{-} antibody-secreting cells and
553 CD20^{+} IgM^{-} IgD^{-} CD10^{-} isotype-switched B cells within all B cells (top) and T-Ag-specific B cells
554 (bottom) in MCC patient samples. Isotype-switched non-antibody-secreting cells were further
555 subdivided into CD27^{+} memory B cells, CD11c^{+} memory B cells, and CD71^{+} activated B cells. **G**.
556 Pooled data from five experiments showing the % of each cell subtype with the population of total B
557 cells from blood of female (top, n=20) or male (bottom, n=27) patients and age-matched controls with
558 no history of MCC (n=5-6). Data from progressor and non-progressor cohorts is displayed separately
559 and combined. **H**. Pooled data from 4 experiments displaying the % of T-Ag-specific B cells within listed
560 B cell subtype. Bars in **G** and **H** represent medians and p values determined by non-parametric Dunn's
561 multiple comparison test are displayed when significant.
562

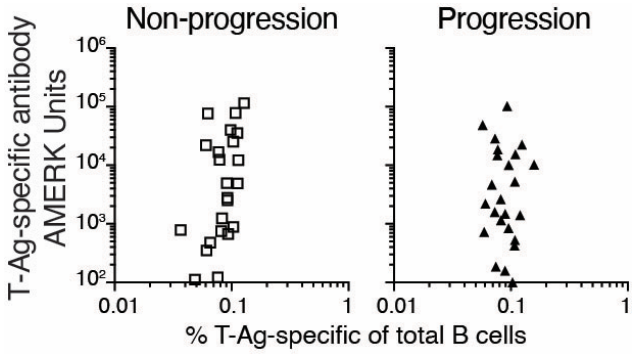

563
564 **Supplemental Figure 3. The frequency of T-Ag-specific B cells in the blood does not associate**
565 **with levels of T-Ag-specific antibodies in the blood or outcome.**
566 Analysis of % of B cells specific for T-Ag in the blood versus the level of T-Ag-specific antibodies in the
567 blood prior to treatment for MCC in patients who did not later experience a progression (left) and
568 patients who experienced progression (right).
569

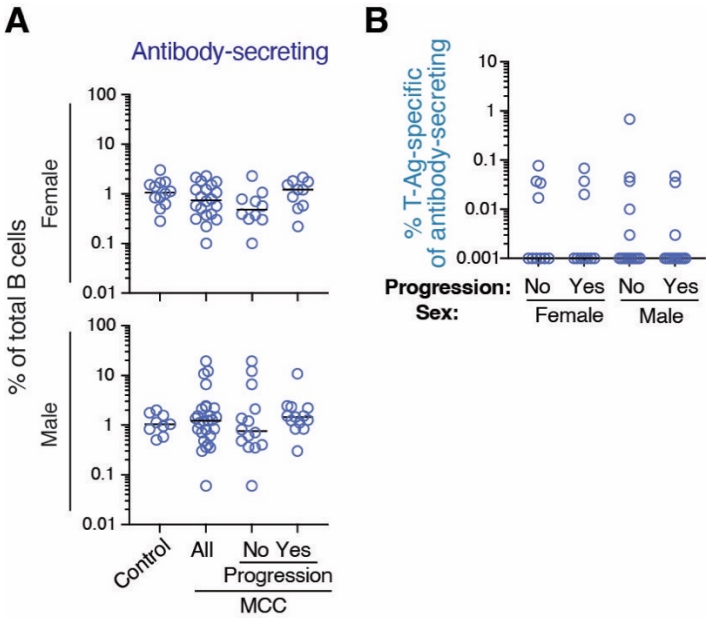

570
571 **Supplemental Figure 4. Increases in antibody-secreting cells associates with MCC progression.**
572 **A**. Pooled data from four experiments showing the % of CD19^{+} CD27^{++} CD20^{-} CD10^{-} antibody-
573 secreting cells with the population of total B cells (top) or % of T-Ag-specific B cells (bottom) found in
574 PBMC from MCC patients prior to treatment. Data from all patients is displayed combined and stratified
575 based upon whether the patient experienced MCC progression after the analysis time point. **B**. Pooled
576 data from four experiments showing the % of T-Ag-specific cells within the total population of antibody-

secreting cells stratified based upon whether the patient experienced MCC progression. Significant p values were generated using a non-parametric Spearman's correlation test. The bars represent the median and p values calculated using a non-parametric Dunn's multiple comparison test are displayed when significant.

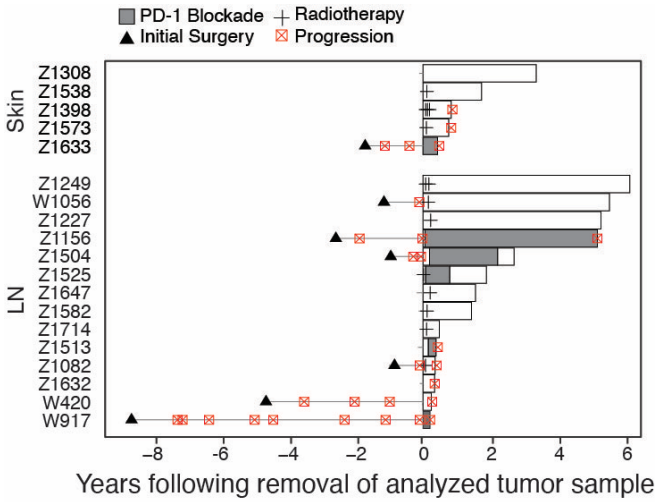

Supplemental Figure 5. Tumor sample cohort patient history summaries.

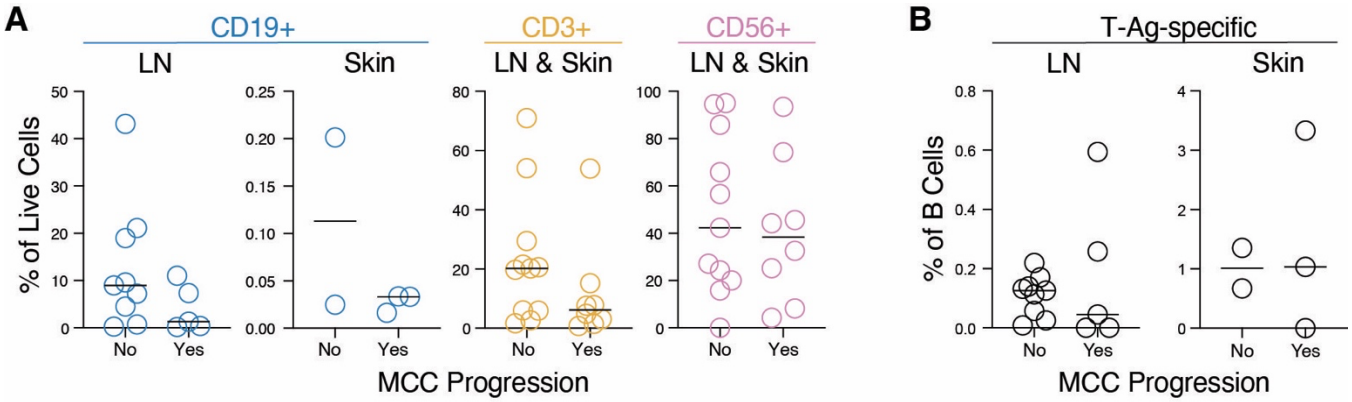

Supplemental Figure 6. Overall Frequency of T cells, B cells, and MCC cells in tumor samples does not associate with MCC progression after treatment.

A. Pooled data from five experiments showing displaying the % of live cells that were CD19$^+$ B cells, CD3$^+$ T cells and CD56$^+$ MCC cells found in MCC skin and LN tumor samples using flow cytometry stratified by based on whether the patient experienced MCC progression during the four-year monitoring period. **B**. Pooled data from five experiments showing displaying the % of CD19$^+$ B cells that were T-Ag-specific found in MCC skin and LN tumor samples stratified based on whether the patient experienced MCC progression during the four-year monitoring period.

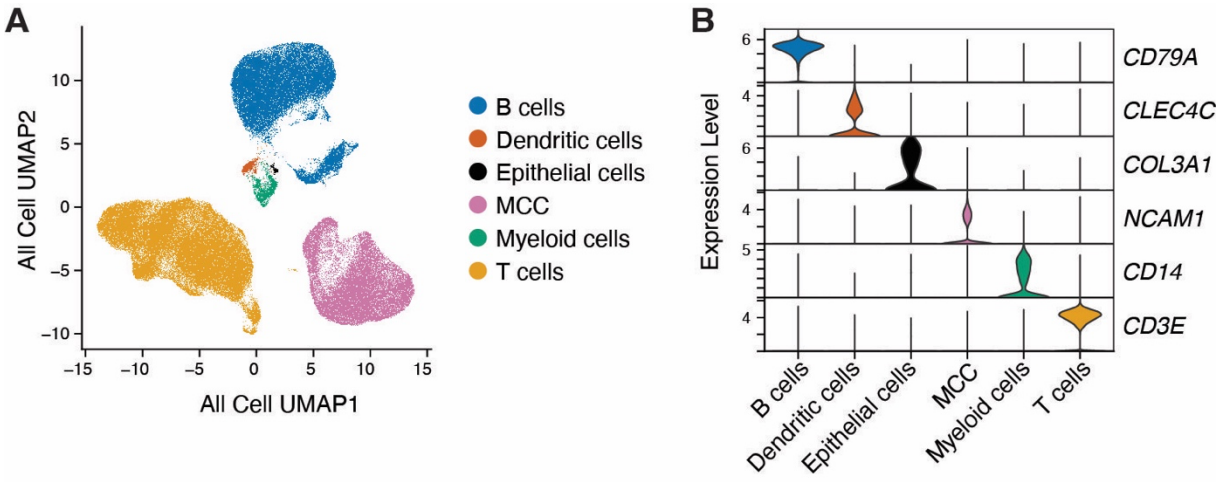

Supplemental Figure 7. Identification of cell types in UMAP clusters.
Expression of key genes used to identify subsets of CD19+ B cells, CD3+ T cells, CD56+ MCC, and a few other contaminating cell types that were not fully excluded during FACS-purification.

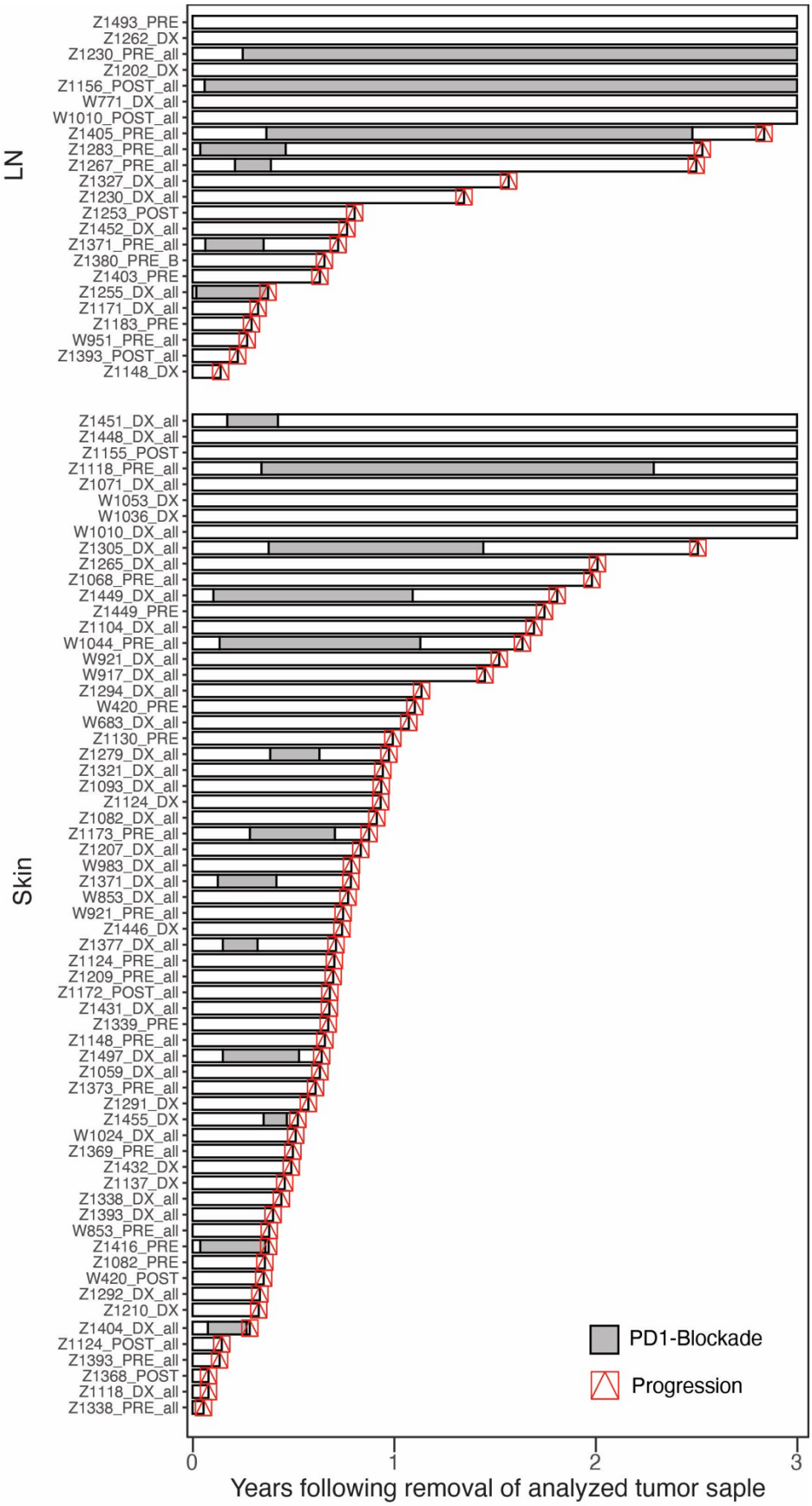

Supplemental Figure 8. Tumor mIHC cohort patient history summaries.

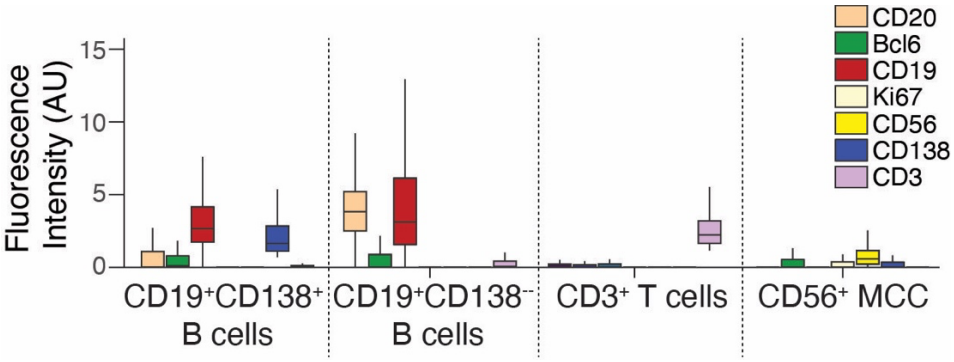

603
604 **Supplemental Figure 9. Staining intensity of markers included in the Tumor mIHC panel.**
605 Staining intensity of markers used in mIHC experiments are displayed for the identified cell subsets.
606

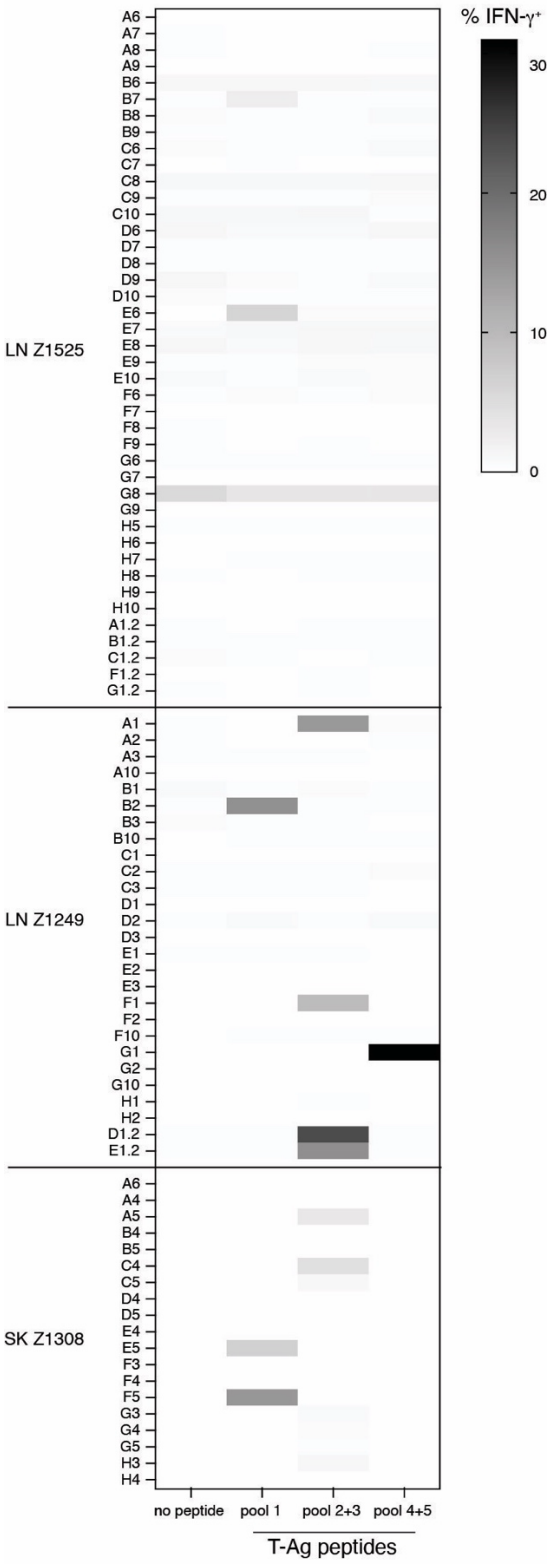

Supplemental Figure 10. Full TCR Screening.
Sixty-nine clonal T_{FH} TCRs from MCC tumor samples were expressed via lentivirus in $CD4^+$ cells from blood and incubated with sample-matched B cells in the absence or presence of 0.1 or 5 μg/mL of T-Ag peptide pools for three days prior to assessment of supernatant for secreted IFNγ. Representative of two similar experiments.

613 **Literature Cited**

614 1. Nghiem, P., Kaufman, H.L., Bharmal, M., Mahnke, L., Phatak, H., and Becker, J.C. (2017).
615 Systematic literature review of efficacy, safety and tolerability outcomes of chemotherapy
616 regimens in patients with metastatic Merkel cell carcinoma. Future oncology *13*, 1263-1279.
617 10.2217/fon-2017-0072.
618 2. Chan, I.S., Bhatia, S., Kaufman, H.L., and Lipson, E.J. (2018). Immunotherapy for Merkel cell
619 carcinoma: a turning point in patient care. J Immunother Cancer *6*, 23. 10.1186/s40425-018-
620 0335-9.
621 3. Albores-Saavedra, J., Batich, K., Chable-Montero, F., Sagy, N., Schwartz, A.M., and Henson,
622 D.E. (2010). Merkel cell carcinoma demographics, morphology, and survival based on 3870
623 cases: a population based study. J Cutan Pathol *37*, 20-27. 10.1111/j.1600-0560.2009.01370.x.
624 4. McEvoy, A.M., Lachance, K., Hippe, D.S., Cahill, K., Moshiri, Y., Lewis, C.W., Singh, N., Park,
625 S.Y., Thuesmunn, Z., Cook, M.M., et al. (2022). Recurrence and Mortality Risk of Merkel Cell
626 Carcinoma by Cancer Stage and Time From Diagnosis. JAMA Dermatol *158*, 382-389.
627 10.1001/jamadermatol.2021.6096.
628 5. Feng, H., Shuda, M., Chang, Y., and Moore, P.S. (2008). Clonal integration of a polyomavirus in
629 human Merkel cell carcinoma. Science *319*, 1096-1100. 10.1126/science.1152586.
630 6. Shuda, M., Arora, R., Kwun, H.J., Feng, H., Sarid, R., Fernandez-Figueras, M.T., Tolstov, Y.,
631 Gjoerup, O., Mansukhani, M.M., Swerdlow, S.H., et al. (2009). Human Merkel cell polyomavirus
632 infection I. MCV T antigen expression in Merkel cell carcinoma, lymphoid tissues and lymphoid
633 tumors. International journal of cancer *125*, 1243-1249. 10.1002/ijc.24510.
634 7. Sastre-Garau, X., Peter, M., Avril, M.F., Laude, H., Couturier, J., Rozenberg, F., Almeida, A.,
635 Boitier, F., Carlotti, A., Couturaud, B., and Dupin, N. (2009). Merkel cell carcinoma of the skin:
636 pathological and molecular evidence for a causative role of MCV in oncogenesis. J Pathol *218*,
637 48-56. 10.1002/path.2532.
638 8. Ryu, H., Bi, T.M., Pulliam, T.H., Sarkar, K., Church, C.D., Kumar, N., Mayer-Blackwell, K., Jani,
639 S., Ramchurren, N., Hansen, U.K., et al. (2024). Merkel cell polyomavirus-specific and
640 CD39(+)CLA(+) CD8 T cells as blood-based predictive biomarkers for PD-1 blockade in Merkel
641 cell carcinoma. Cell Rep Med *5*, 101390. 10.1016/j.xcrm.2023.101390.
642 9. Pulliam, T., Jani, S., Jing, L., Ryu, H., Jojic, A., Shasha, C., Zhang, J., Kulikauskas, R., Church,
643 C., Garnett-Benson, C., et al. (2024). Circulating cancer-specific CD8 T cell frequency is
644 associated with response to PD-1 blockade in Merkel cell carcinoma. Cell Rep Med *5*, 101412.
645 10.1016/j.xcrm.2024.101412.
646 10. Hansen, U.K., Church, C.D., Carnaz Simoes, A.M., Frej, M.S., Bentzen, A.K., Tvingsholm, S.A.,
647 Becker, J.C., Fling, S.P., Ramchurren, N., Topalian, S.L., et al. (2024). T antigen-specific CD8+
648 T cells associate with PD-1 blockade response in virus-positive Merkel cell carcinoma. J Clin
649 Invest *134*. 10.1172/JCI177082.
650 11. Jing, L., Ott, M., Church, C.D., Kulikauskas, R.M., Ibrani, D., Iyer, J.G., Afanasiev, O.K.,
651 Colunga, A., Cook, M.M., Xie, H., et al. (2020). Prevalent and Diverse Intratumoral Oncoprotein-
652 Specific CD8(+) T Cells within Polyomavirus-Driven Merkel Cell Carcinomas. Cancer
653 immunology research *8*, 648-659. 10.1158/2326-6066.CIR-19-0647.
654 12. Paulson, K.G., Carter, J.J., Johnson, L.G., Cahill, K.W., Iyer, J.G., Schrama, D., Becker, J.C.,
655 Madeleine, M.M., Nghiem, P., and Galloway, D.A. (2010). Antibodies to merkel cell
656 polyomavirus T antigen oncoproteins reflect tumor burden in merkel cell carcinoma patients.
657 Cancer research *70*, 8388-8397. 10.1158/0008-5472.CAN-10-2128.
658 13. Paulson, K.G., Lewis, C.W., Redman, M.W., Simonson, W.T., Lisberg, A., Ritter, D., Morishima,
659 C., Hutchinson, K., Mudgistratova, L., Blom, A., et al. (2017). Viral oncoprotein antibodies as a
660 marker for recurrence of Merkel cell carcinoma: A prospective validation study. Cancer *123*,
661 1464-1474. 10.1002/cncr.30475.
662 14. Miller, N.J., Church, C.D., Fling, S.P., Kulikauskas, R., Ramchurren, N., Shinohara, M.M.,
663 Kluger, H.M., Bhatia, S., Lundgren, L., Cheever, M.A., et al. (2018). Merkel cell polyomavirus-

664 specific immune responses in patients with Merkel cell carcinoma receiving anti-PD-1 therapy. J
665 Immunother Cancer *6*, 131. 10.1186/s40425-018-0450-7.
666 15. Schumacher, T.N., and Schreiber, R.D. (2015). Neoantigens in cancer immunotherapy. Science
667 *348*, 69-74. 10.1126/science.aaa4971.
668 16. Lahman, M.C., Paulson, K.G., Nghiem, P.T., and Chapuis, A.G. (2021). Quality Is King:
669 Fundamental Insights into Tumor Antigenicity from Virus-Associated Merkel Cell Carcinoma.
670 The Journal of investigative dermatology *141*, 1897-1905. 10.1016/j.jid.2020.12.037.
671 17. Yang, Y., Chen, X., Pan, J., Ning, H., Zhang, Y., Bo, Y., Ren, X., Li, J., Qin, S., Wang, D., et al.
672 (2024). Pan-cancer single-cell dissection reveals phenotypically distinct B cell subtypes. Cell
673 *187*, 4790-4811 e4722. 10.1016/j.cell.2024.06.038.
674 18. Fitzsimons, E., Qian, D., Enica, A., Thakkar, K., Augustine, M., Gamble, S., Reading, J.L., and
675 Litchfield, K. (2024). A pan-cancer single-cell RNA-seq atlas of intratumoral B cells. Cancer Cell
676 *42*, 1784-1797 e1784. 10.1016/j.ccell.2024.09.011.
677 19. Ma, J., Wu, Y., Ma, L., Yang, X., Zhang, T., Song, G., Li, T., Gao, K., Shen, X., Lin, J., et al.
678 (2024). A blueprint for tumor-infiltrating B cells across human cancers. Science *384*, eadj4857.
679 10.1126/science.adj4857.
680 20. Cui, C., Wang, J., Fagerberg, E., Chen, P.M., Connolly, K.A., Damo, M., Cheung, J.F., Mao, T.,
681 Askari, A.S., Chen, S., et al. (2021). Neoantigen-driven B cell and CD4 T follicular helper cell
682 collaboration promotes anti-tumor CD8 T cell responses. Cell *184*, 6101-6118 e6113.
683 10.1016/j.cell.2021.11.007.
684 21. Wieland, A., Patel, M.R., Cardenas, M.A., Eberhardt, C.S., Hudson, W.H., Obeng, R.C., Griffith,
685 C.C., Wang, X., Chen, Z.G., Kissick, H.T., et al. (2021). Defining HPV-specific B cell responses
686 in patients with head and neck cancer. Nature *597*, 274-278. 10.1038/s41586-020-2931-3.
687 22. Eberhardt, C.S., Kissick, H.T., Patel, M.R., Cardenas, M.A., Prokhnevska, N., Obeng, R.C.,
688 Nasti, T.H., Griffith, C.C., Im, S.J., Wang, X., et al. (2021). Functional HPV-specific PD-1(+)
689 stem-like CD8 T cells in head and neck cancer. Nature *597*, 279-284. 10.1038/s41586-021-
690 03862-z.
691 23. Taylor, J.J., Martinez, R.J., Titcombe, P.J., Barsness, L.O., Thomas, S.R., Zhang, N., Katzman,
692 S.D., Jenkins, M.K., and Mueller, D.L. (2012). Deletion and anergy of polyclonal B cells specific
693 for ubiquitous membrane-bound self-antigen. The Journal of experimental medicine *209*, 2065-
694 2077. 10.1084/jem.20112272.
695 24. Phelps, A., Pazos-Castro, D., Urselli, F., Grydziuszko, E., Mann-Delany, O., Fang, A., Walker,
696 T.D., Guruge, R.T., Tome-Amat, J., Diaz-Perales, A., et al. (2024). Production and use of
697 antigen tetramers to study antigen-specific B cells. Nat Protoc *19*, 727-751. 10.1038/s41596-
698 023-00930-8.
699 25. Starrett, G.J., Thakuria, M., Chen, T., Marcelus, C., Cheng, J., Nomburg, J., Thorner, A.R.,
700 Slevin, M.K., Powers, W., Burns, R.T., et al. (2020). Clinical and molecular characterization of
701 virus-positive and virus-negative Merkel cell carcinoma. Genome Med *12*, 30. 10.1186/s13073-
702 020-00727-4.
703 26. Houben, R., Adam, C., Baeurle, A., Hesbacher, S., Grimm, J., Angermeyer, S., Henzel, K.,
704 Hauser, S., Elling, R., Brocker, E.B., et al. (2012). An intact retinoblastoma protein-binding site
705 in Merkel cell polyomavirus large T antigen is required for promoting growth of Merkel cell
706 carcinoma cells. International journal of cancer *130*, 847-856. 10.1002/ijc.26076.
707 27. Cheng, J., Rozenblatt-Rosen, O., Paulson, K.G., Nghiem, P., and DeCaprio, J.A. (2013). Merkel
708 cell polyomavirus large T antigen has growth-promoting and inhibitory activities. J Virol *87*,
709 6118-6126. 10.1128/JVI.00385-13.
710 28. Ortiz, L.E., Pham, A.M., and Kwun, H.J. (2021). Identification of the Merkel Cell Polyomavirus
711 Large Tumor Antigen Ubiquitin Conjugation Residue. Int J Mol Sci *22*. 10.3390/ijms22137169.
712 29. Houben, R., Shuda, M., Weinkam, R., Schrama, D., Feng, H., Chang, Y., Moore, P.S., and
713 Becker, J.C. (2010). Merkel cell polyomavirus-infected Merkel cell carcinoma cells require
714 expression of viral T antigens. J Virol *84*, 7064-7072. 10.1128/JVI.02400-09.

715 30. Shuda, M., Kwun, H.J., Feng, H., Chang, Y., and Moore, P.S. (2011). Human Merkel cell
716 polyomavirus small T antigen is an oncoprotein targeting the 4E-BP1 translation regulator. J
717 Clin Invest *121*, 3623-3634. 10.1172/JCI46323.
718 31. Peckham, H., Radziszewska, A., Sikora, J., de Gruijter, N.M., Restuadi, R., Kartawinata, M.,
719 Martin-Gutierrez, L., Robinson, G.A., Deakin, C.T., Wedderburn, L.R., et al. (2025). Estrogen
720 influences class-switched memory B cell frequency only in humans with two X chromosomes.
721 The Journal of experimental medicine *222*. 10.1084/jem.20241253.
722 32. McEvoy, A.M., Hippe, D.S., Lachance, K., Park, S., Cahill, K., Redman, M., Gooley, T., Kattan,
723 M.W., and Nghiem, P. (2024). Merkel cell carcinoma recurrence risk estimation is improved by
724 integrating factors beyond cancer stage: A multivariable model and web-based calculator.
725 Journal of the American Academy of Dermatology *90*, 569-576. 10.1016/j.jaad.2023.11.020.
726 33. Becht, E., McInnes, L., Healy, J., Dutertre, C.A., Kwok, I.W.H., Ng, L.G., Ginhoux, F., and
727 Newell, E.W. (2018). Dimensionality reduction for visualizing single-cell data using UMAP.
728 Nature biotechnology. 10.1038/nbt.4314.
729 34. Nakamura, M., Magara, T., Kano, S., Matsubara, A., Kato, H., and Morita, A. (2022). Tertiary
730 Lymphoid Structures and Chemokine Landscape in Virus-Positive and Virus-Negative Merkel
731 Cell Carcinoma. Front Oncol *12*, 811586. 10.3389/fonc.2022.811586.
732 35. Nakamura, M., Yoshimitsu, M., Magara, T., Kano, S., Kato, H., and Morita, A. (2024). Analyses
733 of tertiary lymphoid structures observed in cases of Merkel cell carcinoma showing spontaneous
734 regression. Exp Dermatol *33*, e15062. 10.1111/exd.15062.
735 36. Behr, D.S., Peitsch, W.K., Hametner, C., Lasitschka, F., Houben, R., Schonhaar, K., Michel, J.,
736 Dollt, C., Goebeler, M., Marx, A., et al. (2014). Prognostic value of immune cell infiltration,
737 tertiary lymphoid structures and PD-L1 expression in Merkel cell carcinomas. Int J Clin Exp
738 Pathol *7*, 7610-7621.
739 37. Veatch, J.R., Lee, S.M., Shasha, C., Singhi, N., Szeto, J.L., Moshiri, A.S., Kim, T.S., Smythe,
740 K., Kong, P., Fitzgibbon, M., et al. (2022). Neoantigen-specific CD4(+) T cells in human
741 melanoma have diverse differentiation states and correlate with CD8(+) T cell, macrophage,
742 and B cell function. Cancer Cell *40*, 393-409 e399. 10.1016/j.ccell.2022.03.006.
743 38. Moffett, H.F., Harms, C.K., Fitzpatrick, K.S., Tooley, M.R., Boonyaratanakornkit, J., and Taylor,
744 J.J. (2019). B cells engineered to express pathogen-specific antibodies protect against infection.
745 Science immunology *4*. 10.1126/sciimmunol.aax0644.
746 39. Koerber, J.T., Hornsby, M.J., and Wells, J.A. (2015). An improved single-chain Fab platform for
747 efficient display and recombinant expression. J Mol Biol *427*, 576-586.
748 10.1016/j.jmb.2014.11.017.
749 40. Schmidt, T.G., Koepke, J., Frank, R., and Skerra, A. (1996). Molecular interaction between the
750 Strep-tag affinity peptide and its cognate target, streptavidin. J Mol Biol *255*, 753-766.
751 10.1006/jmbi.1996.0061.
752 41. Voss, S., and Skerra, A. (1997). Mutagenesis of a flexible loop in streptavidin leads to higher
753 affinity for the Strep-tag II peptide and improved performance in recombinant protein
754 purification. Protein Eng *10*, 975-982. 10.1093/protein/10.8.975.
755 42. Schmidt, T.G., and Skerra, A. (2007). The Strep-tag system for one-step purification and high-
756 affinity detection or capturing of proteins. Nat Protoc *2*, 1528-1535. 10.1038/nprot.2007.209.
757 43. Montero-Calle, A., Garranzo-Asensio, M., Moreno-Casbas, M.T., Campuzano, S., and
758 Barderas, R. (2024). Autoantibodies in cancer: a systematic review of their clinical role in the
759 most prevalent cancers. Frontiers in immunology *15*, 1455602. 10.3389/fimmu.2024.1455602.
760 44. Laumont, C.M., Banville, A.C., Gilardi, M., Hollern, D.P., and Nelson, B.H. (2022). Tumour-
761 infiltrating B cells: immunological mechanisms, clinical impact and therapeutic opportunities. Nat
762 Rev Cancer *22*, 414-430. 10.1038/s41568-022-00466-1.
763 45. Lounici, Y., Le Saux, O., Chemin, G., Wajda, P., Barrin, S., Berthet, J., Caux, C., and Dubois, B.
764 (2022). Heterogeneity and Functions of Tumor-Infiltrating Antibody Secreting Cells: Lessons
765 from Breast, Ovarian, and Other Solid Cancers. Cancers (Basel) *14*. 10.3390/cancers14194800.

766 46. Alspach, E., Lussier, D.M., Miceli, A.P., Kizhvatov, I., DuPage, M., Luoma, A.M., Meng, W.,
767 Lichti, C.F., Esaulova, E., Vomund, A.N., et al. (2019). MHC-II neoantigens shape tumour
768 immunity and response to immunotherapy. Nature *574*, 696-701. 10.1038/s41586-019-1671-8.
769 47. Zander, R., Schauder, D., Xin, G., Nguyen, C., Wu, X., Zajac, A., and Cui, W. (2019). CD4(+) T
770 Cell Help Is Required for the Formation of a Cytolytic CD8(+) T Cell Subset that Protects against
771 Chronic Infection and Cancer. Immunity *51*, 1028-1042 e1024. 10.1016/j.immuni.2019.10.009.
772 48. Verhaegen, M.E., Harms, P.W., Van Goor, J.J., Arche, J., Patrick, M.T., Wilbert, D., Zabawa, H.,
773 Grachtchouk, M., Liu, C.J., Hu, K., et al. (2022). Direct cellular reprogramming enables
774 development of viral T antigen-driven Merkel cell carcinoma in mice. J Clin Invest *132*.
775 10.1172/JCI152069.
776 49. McLellan, J.S., Chen, M., Joyce, M.G., Sastry, M., Stewart-Jones, G.B., Yang, Y., Zhang, B.,
777 Chen, L., Srivatsan, S., Zheng, A., et al. (2013). Structure-based design of a fusion glycoprotein
778 vaccine for respiratory syncytial virus. Science *342*, 592-598. 10.1126/science.1243283.
779 50. Fitzpatrick, K.S., Degefu, H.N., Poljakov, K., Bibby, M.G., Remington, A.J., Searles, T.G., Gray,
780 M.D., Boonyaratanakornkit, J., Rosato, P.C., and Taylor, J.J. (2023). Validation of Ligand
781 Tetramers for the Detection of Antigen-Specific Lymphocytes. J Immunol *210*, 1156-1165.
782 10.4049/jimmunol.2200934.
783

METHODS

RESOURCE AVAILABILITY

Lead contact

Further information and requests for resources and reagents should be directed to and will be fulfilled by the lead contacts, Paul Nghiem (pnghiem@uw.edu) and/or Justin Taylor (justintaylor@virginia.edu)

Materials availability

Available upon request.

Data and code availability

The expression data obtained in this study has been uploaded to the GEO database with accession no. GSE301498. Any requests for the raw data will be reviewed by the corresponding authors to ensure patient confidentiality is maintained. If possible, the data will be shared under a material transfer agreement. This paper does not report original code, however, code needed to reproduce any of the analyses will be made available upon reasonable request. Any additional information required to reanalyze the data reported in this work is available from the lead contacts upon request.

EXPERIMENTAL MODEL AND SUBJECT DETAILS

Mouse Studies

Animal studies were approved and conducted in accordance with the Fred Hutchinson Cancer Center Institutional Animal Care and Use Committee. Six- to ten-week-old female C57BL/6 mice were obtained from the Jackson Laboratory.

Human Studies

Blood samples from MCC patients (**Figure S1, Table S2**) were collected with informed consent for research use and were approved by the Fred Hutchinson Cancer Center (FHCC) institutional review board, in accordance with the Declaration of Helsinki (2013) as part of observational registry studies focusing on Merkel cell carcinoma (IRB protocol 6585). Titers of T-Ag-specific antibodies in blood were determined by the Clinical Immunology Lab at Department of Laboratory Medicine and Pathology at the University of Washington using the AMERK test[13]. Patient samples were selected based on availability of frozen viable PBMCs collected within 67 days of MCC diagnosis. In addition, patient samples were selected to be representative of the sex distribution observed in virally driven MCC. Patient samples were further selected to only include MCPyV-positive cases and those from immune competent patients. Blood samples from age-matched, non-MCC controls were collected with informed consent for research use and were approved by the University of Washington institutional review board, in accordance with the Declaration of Helsinki (2013) (IRB protocol STUDY00001399).

Tumor samples from MCC patients (**Figure S5, S8, Tables S3, S7**) were collected with informed consent for research use and were approved by the Fred Hutchinson Cancer Center (FHCC) institutional review board, in accordance with the Declaration of Helsinki (2013) as part of observational registry studies focusing on Merkel cell carcinoma (IRB protocol 6585). Additionally, tumor samples for single cell experiments (**Figure S5, Table S3**) were selected based on availability of frozen viable tumor digests, number of cells available in sample (>10 million), and included only MCPyV-positive cases. Patient samples were primarily from males due to limited female tumor samples.

Recurrence risk of MCC PBMC patient cohort (**Figure S1, Table S2**) was calculated using an open-source MCC recurrence risk calculator (https://merkelcell.org/prognosis/recur/)[4]. This calculator estimates the probability of recurrence from the time of diagnosis in patients with no prior presentation of MCC. Briefly, percent probability of recurrence for each patient following MCC diagnosis was calculated using known risk factors including age, sex, stage as defined by the American Joint Committee on Cancer, site of primary tumor, and immune status. In contrast, because some MCC patients in single cell RNA-sequencing tumor cohort had prior disease recurrences (**Figure S5, Table S3**), clinical recurrence risk in these patients was independently assessed by 3 blinded clinicians. Known risk factors used for this assessment included age, sex, MCC stage, presence of metastatic

837 disease, prior recurrences, and immune status. Each patient was then categorized as having
838 "Medium/Low" or "High" probability of MCC recurrence following surgical excision of analyzed tumor.
839 To assess long-term MCC outcomes in blood studies (**Figure S1, Table S2**), patients were
840 monitored for 3 years starting at the time of biopsy-proven MCC diagnosis. For progression-free
841 survival analyses, an event consisted of a patient having a recurrence or progression of MCC following
842 definitive treatment (surgery, radiation, or anti-PD1 immunotherapy alone or in combination). Patients
843 with no MCC recurrences were censored following 3 years of follow-up.
844 To assess long-term MCC outcomes in single cell RNA-sequencing tumor studies (**Figure S5,**
845 **Table S3**) and in tumor imaging studies (**Figure S8, Table S7**), patients were monitored for 4 and 3
846 years, respectively, starting at the time surgical excision of analyzed tumor. For progression-free
847 survival analyses, an event consisted of a patient having a recurrence or progression of MCC following
848 definitive treatment (surgery, radiation, or anti-PD1 immunotherapy alone or in combination). Patients
849 with no MCC progression were censored following the monitoring period for each study.
850
851 **METHOD DETAILS**
852 Production of T-Ag, GST, and RSV F proteins
853 Production of the common T-Ag domain shared by both small and large T-Ag isoforms, was
854 performed as previously described[12]. Briefly, pGEX4T3 plasmids (GE Healthcare) encoding the T-Ag
855 fused to glutathione S-transferase (GST) or GST alone were expressed in Rosetta Escherichia coli and
856 harvested by centrifugation 15 h after induction. Pelleted bacteria were resuspended in 40 mM Tris pH
857 8.0, 200 mM NaCl, 1 mM EDTA, and 2 mM DTT supplemented with complete protease inhibitor cocktail
858 and lysed by two passes through a Microfluidizer. Lysates were then diluted with an equal volume of
859 glycerol. Pierce Glutathione Spin Columns (ThermoFisher) were used following manufacturer's
860 instructions to purify GST and T-Ag. After purification, proteins were buffer exchanged by centrifugation
861 using 10kDa Amicon Ultra centrifugal filters into 1xDPBS, aliquoted at 40 μM concentrations, and run
862 on SDS-PAGE to assess protein purification.
863 Expression plasmid for His-tagged RSV prefusion F antigen was previously described[49]. Briefly,
864 293F cells were transfected at a density of 10^6 cells/mL in Freestyle 293 media using 1 mg/mL PEI Max
865 (Polysciences). Transfected cells were cultured for 7 days with gentle shaking at 37 °C. Supernatant
866 was collected by centrifuging cultures at 2500×*g* for 30 minutes followed by filtration through a 0.2 μM
867 filter. The clarified supernatant was incubated with Ni Sepharose beads overnight at 4 °C, followed by
868 washing with wash buffer containing 50 mM Tris, 300 mM NaCl, and 8 mM imidazole. His-tagged
869 protein was eluted with an elution buffer containing 25 mM Tris, 150 mM NaCl, and 500 mM imidazole.
870 The purified protein was run over a 10/300 Superose 6 size exclusion column (GE Life Sciences).
871 Fractions containing the trimeric F protein were pooled and concentrated using 50 kDa Amicon Ultra
872 centrifugal filters (Millipore). The concentrated sample was stored in 50% glycerol at −20 °C.
873
874 Production of T-Ag and control tetramers
875 Production of T-Ag, GST, and RSV F tetramers was performed using a previously described
876 protocol[23,24]. Briefly, purified T-Ag, GST, and RSV F proteins were biotinylated using the EZ-Link Sulfo-
877 NHS-LC Biotinylation kit according to manufacturer instructions. Following biotinylation reaction, excess
878 biotin was removed by centrifugation using 10 kDa Amicon Ultra centrifugal filters. Next, the molar ratio
879 of biotin:protein was assessed by Western blot and selected to be ~1:1 to prevent over- or under-
880 biotinylation of antigen that could reduce the downstream efficacy of protein tetramers. After
881 optimization of biotinylation, T-Ag, GST, and RSV F tetramers were assembled by incubating
882 biotinylated protein with either streptavidin-APC or streptavidin-PE at a 4:1 molar ratio of
883 protein:streptavidin for 30 minutes at room temperature and in the dark. Unconjugated T-Ag and GST
884 were removed by centrifugation using 100 kDa Amicon Ultra centrifugal filters, whereas unconjugated
885 RSV F was removed also by centrifugation but using a 300 K Nanosep centrifugal device (Pall
886 Corporation). Tetramers were buffer exchanged into 1xDPBS by centrifugation using 100 kDa Amicon
887 Ultra centrifugal filter and diluted to 1 μM in 50% glycerol in 1xDPBS for long-term storage at -20C.
888 To make control tetramers, streptavidin-PE was conjugated to DyLight 594 (PE594) or DyLight 650
889 (PE650), and streptavidin-APC conjugated to DyLight 755 (APC755) using the DyLight Antibody

890 Labeling kit following manufacturer instructions. After removal of excess dye by centrifugation using
891 10kDa Amicon Ultra centrifugal filters, biotinylated GST was incubated with streptavidin-PE594 or
892 streptavidin-APC755 at a 4:1 ratio of protein:streptavidin for 30 minutes at room temperature and in the
893 dark. Control tetramers were diluted to 1-3 μM in 50% glycerol diluted with 1xDPBS for long-term
894 storage at -20C.
895 Oligo-barcoded tetramers were assembled using TotalSeq-C streptavidin-PE. Briefly, biotinylated T-
896 Ag, biotinylated GST-DL594, and biotinylated RSV F were incubated with TotalSeq-C streptavidin-PE
897 containing uniquely identifying oligo tags at a molar 4:1 ratio of protein:streptavidin for 30 minutes at
898 room temperature and in the dark. Unconjugated T-Ag and GST were removed by centrifugation using
899 100 kDa Amicon Ultra centrifugal filters, whereas unconjugated RSV F was removed also by
900 centrifugation but using a 300 K Nanosep centrifugal device (Pall Corporation).
901
902 Enrichment and analysis of tetramer-binding mouse B cells
903 Six- to ten-week-old C57BL/6J female mice were used for experiments. Mice were injected
904 intraperitoneally with 50 μL of CFA emulsion containing 5 μg of T-Ag in 1xDPBS or 1xDPBS alone as
905 control. Seven days post-vaccination, tetramer-binding B cells were enriched using a previously
906 described protocol[23,24]. Briefly, the spleen inguinal, axillary, brachial, cervical, mesenteric, and periaortic
907 lymph nodes for each mouse were pooled and manually dissociated. Following dissociation, 10 mL of
908 DPBS containing 1% heat-inactivated newborn calf serum (sorting buffer) was added, and tissue debris
909 removed, the samples pelleted, and supernatant discarded. For staining of T-Ag-specific B cells, each
910 sample was first incubated with 1 pmol of PE594 control tetramer, 3 pmol of APC755 control tetramer,
911 and 2 μg of anti-Fc receptor antibody 2.4G2 (BioXcell) in 0.2 mL sorting buffer for 10 minutes on ice.
912 Next, 1 pmol GST APC tetramer, 1 pmol T-Ag PE tetramer, a cell viability dye and fluorescent
913 antibodies against cell-surface lineage markers (CD3, F4/80, Gr-1, B220, CD38, and GL7) were added
914 to samples followed by incubation on ice for 25 minutes. After the incubation, ~10 mL of sorting buffer
915 was added and the samples centrifuged at 300 × g for five minutes at 4°C and supernatant discarded.
916 Cells were resuspended in 0.15 mL sorting buffer containing 25 μL of anti-APC and 25 μL of anti-PE
917 conjugated microbeads (Miltenyi) and incubated for 30 minutes on ice. Next, 5 mL of sorting buffer was
918 added to each sample and passed over a magnetized LS column (Miltenyi). The tube and column were
919 washed once with 5 mL of sorting buffer and then removed from the magnetic field. Five mL of sorting
920 buffer was pushed through the column with a plunger to elute column-bound cells. Another 5 mL of
921 sorting buffer was plunged through the column to maximize recovery.
922 For intracellular staining, cells were fixed and permeabilized using the BD Cytofix/Cytoperm buffer
923 according to manufacturer's instructions. Following permeabilization, an anti-mouse Ig was added and
924 samples incubated for 30 minutes on ice. After incubation, ~4 mL of sorting buffer was added and the
925 samples centrifuged at 300 × g for five minutes at 4°C and supernatant discarded. Samples were
926 resuspended sorting buffer containing 20,000 AccuCheck Counting Beads (ThermoFisher) analyzed by
927 the BD Fortessa flow cytometer at the Fred Hutch Cancer Center's Flow Core Facility. UltraComp
928 eBeads Plus (ThermoFisher) or splenocytes were used as single stained controls. Compensation
929 matrix was set up using the BD FACSDiva software. Analysis performed using FlowJo v.10.10.
930
931 Enrichment and sorting of T-Ag-specific B cells from human blood
932 Heparinized whole blood from MCC patients was processed at the Specimen Processing Lab (Fred
933 Hutch Cancer Center). PBMC were isolated by routine Ficoll density gradient centrifugation and
934 cryopreserved in freezing medium [50% human serum (Valley Biomedical), 40% RPMI (Corning), and
935 10% DMSO (Sigma-Aldrich)]. 5-10 × 10^7 frozen PBMCs from MCC patients or non-MCC controls were
936 thawed into DMEM with 10% fetal calf serum and 100 U/mL penicillin. Cells were centrifuged,
937 resuspended in 100 μL of ice-cold sorting buffer containing 1 pmol of GST PE650 tetramers and 2% rat
938 and mouse serum (ThermoFisher), and incubated at on ice for 10 min. Next, 1 pmol of T-Ag PE
939 tetramers were then added at a final concentration of 5 nM and incubated on ice for 25 min, followed by
940 a 10 mL wash with ice-cold sorting buffer. Next, 25 μL each of anti-APC and anti-PE microbeads
941 (Miltenyi) were added and incubated on ice for 30 minutes, after which 3 mL of sorting buffer was
942 added, and the mixture was passed over a magnetized LS column (Miltenyi). The column was washed

943 once with 5 mL ice-cold sorting buffer and then removed from the magnetic field and 5 mL ice-cold
944 sorting buffer was pushed through the unmagnetized column twice using a plunger to elute the bound
945 cell fraction. Cells were then incubated with 50 µL of sorting buffer containing a cell viability dye and
946 fluorescent antibodies against cell-surface lineage markers (CD3, CD14, CD16, and CD19) for 30 min
947 on ice prior to washing and analysis on a BD FACS Aria sorter at the Fred Hutch Cancer Center's Flow
948 Core Facility. UltraComp eBeads Plus (ThermoFisher) or PBMCs were used as single stained controls.
949 Compensation matrix and gating of tetramer-binding B cells was set up using the BD FACSDiva
950 software. Tetramer-binding B cells were then individually sorted into empty 96-well PCR plates and
951 immediately frozen.
952
953 B cell receptor sequencing using single cell RT-PCR
954 As described previously[50], individual B cells sorted and frozen into empty 96-well PCR plates,
955 reverse transcription (RT) was directly performed after thawing plates using SuperScript IV
956 (ThermoFisher). Briefly, 3 µL RT reaction mix consisting of 3 µL of 50 µM random hexamers
957 (ThermoFisher), 0.8 µL of 25 mM deoxyribonucleotide triphosphates (dNTPs; ThermoFisher), 1 µL (20
958 U) SuperScript IV RT, 0.5 µL (20 U) RNaseOUT (ThermoFisher), 0.6 µL of 10% Igepal (Sigma-Aldrich),
959 and 15 µL RNase-free water was added to each well containing a single sorted B cell and incubated at
960 50°C for 1 h. Following RT, 2 µL of cDNA was added to 19 µL PCR reaction mix so that the final
961 reaction contained 0.2 µL (0.5 U) HotStarTaq Polymerase (Qiagen), 0.075 µL of 50 µM 3′ reverse
962 primers, 0.115 µL of 50 µM 5′ forward primers, 0.24 µL of 25 mM dNTPs, 1.9 µL of 10 × buffer (Qiagen),
963 and 16.5 µL of water. The PCR program was 50 cycles of 94°C for 30 s, 57°C for 30 s, and 72°C for
964 55 s, followed by 72°C for 10 min for heavy and kappa light chains. The PCR program was 50 cycles of
965 94°C for 30 s, 60°C for 30 s, and 72°C for 55 s, followed by 72°C for 10 min for lambda light chains.
966 After the first round of PCR, 2 µL of the PCR product was added to 19 µL of the second-round PCR
967 reaction so that the final reaction contained 0.2 µL (0.5 U) HotStarTaq Polymerase, 0.075 µL of 50 µM
968 3′ reverse primers, 0.075 µL of 50 µM 5′ forward primers, 0.24 µL of 25 mM dNTPs, 1.9 µL 10 × buffer,
969 and 16.5 µL of water. PCR programs were the same as the first round of PCR. 4 µL of the PCR product
970 was run on an agarose gel to confirm the presence of a ~500-bp heavy chain band or ~450-bp light
971 chain band. 5 µL from the PCR reactions showing the presence of heavy or light chain amplicons was
972 mixed with 2 µL of ExoSAP-IT (ThermoFisher) and incubated at 37°C for 15 min followed by 80 °C for
973 15 min to hydrolyze excess primers and nucleotides. Hydrolyzed second-round PCR products were
974 sequenced by Genewiz with the respective reverse primer used in the second-round PCR, and
975 sequences were analyzed using IMGT/V-Quest to identify V, D, and J gene segments. Paired heavy
976 chain *VDJ* and light chain *VJ* sequences were cloned into pTT3-derived expression vectors containing
977 the human IgG1, IgK, or IgL constant regions using In-Fusion cloning (Clontech).
978
979 Monoclonal antibody production
980 Secreted T-Ag and control IgG1 antibodies were produced by Genscript, WuXi, or in house as
981 described previously[50]. For the latter, 10^6 cells/mL of 293F cells were co-transfected with heavy and
982 light chain expression plasmids at a ratio of 1:1 in Freestyle 293 media (ThermoFisher) using 1 mg/mL
983 PEI Max. Transfected cells were cultured for 7 days with gentle shaking at 37 °C. Supernatant was
984 collected by centrifuging cultures at 2500×*g* for 15 minutes followed by filtration through a 0.2 µM filter.
985 Clarified supernatants were then incubated with Protein A agarose (ThermoFisher) followed by washing
986 with IgG-binding buffer (ThermoFisher). Antibodies were eluted with IgG Elution Buffer (ThermoFisher)
987 into a neutralization buffer containing 1 M Tris-base pH 9.0. Purified antibody was concentrated and
988 buffer exchanged into 1xDPBS using 50 kDa Amicon Ultra centrifugal filters.
989
990 Bio-Layer Interferometry
991 Bio-layer interferometry (BLI) assays were performed on the Octet.Red instrument (ForteBio) at
992 room temperature with shaking at 500 rpm. To assess binding of monoclonal antibodies to T-Ag,
993 streptavidin capture sensors (ForteBio) were loaded in kinetics buffer (PBS with 0.01% bovine serum
994 albumin, 0.02% Tween 20, and 0.005% NaN_3, pH 7.4) containing 1 µM biotinylated GST as control or
995 biotinylated T-Ag for 2.5 minutes. After loading, the baseline signal was recorded for 1 minute in a
996 kinetics buffer. The sensors were then immersed in kinetics buffer containing 40 µg/mL of purified

997 monoclonal antibody for a five-minute association step followed by immersion in kinetics buffer for a
998 five-minute dissociation phase. The binding curves were generated after subtracting the background
999 signal from each analyte-containing well using a negative control mAb at each time point. Curve fitting
1000 was performed using a 1:1 binding model and ForteBio Octet data analysis software release 9.0.
1001
1002 Spectral flow cytometry of B cells in MCC patient blood
1003 PBMC from MCC patients (**Figure S2, Table S2)** were analyzed by spectral flow cytometry. Briefly,
1004 frozen PBMC were thawed into DMEM with 10% fetal calf serum and 100 U/mL penicillin. Cells were
1005 centrifuged and resuspended in 50 µL of ice-cold sorting buffer. GST APC755 was added at a final
1006 concentration of 1.25 pmol in the presence of 2% rat and mouse serum (ThermoFisher) and incubated
1007 at room temperature for 10 min. Cells were then incubated with 50 µL of sorting buffer containing a cell
1008 viability dye, 0.5 pmol of T-Ag APC tetramer, and fluorescent antibodies against cell-surface lineage
1009 markers (CD3, CD14, CD16, CD19, CD20, CD10, CD27, CD11c, CD71, IgM, IgD, and IgG) for 30 min
1010 on ice prior to washing and analysis on a Cytek Aurora spectral analyzer at the University of
1011 Washington, Department of Immunology's Cell Analysis Facility. Antibody capture beads
1012 (ThermoFisher) or cells were used to compensate each fluorophore in the experiment. Spectral
1013 unmixing was performed using SpectroFlo software. Analysis performed using FlowJo v.10.10.
1014
1015 Tumor single cell RNAseq sample preparation
1016 Fresh MCC tumor specimens from needle cores, punch biopsies, or surgical excisions were
1017 processed into single-cell digests by mincing them into small pieces with sterile forceps and scissors,
1018 followed by incubation in 20 mL of digestion medium composed of RPMI plus 0.002 g DNase
1019 (Worthington Biochemical), 0.008 g collagenase (Worthington Biochemical), and 0.002 g hyaluronidase
1020 (Worthington Biochemical) in a 10-cm dish at 37°C with frequent, gentle swirling. After 3 hours of
1021 digestion, cells were strained through a 70 µm filter, centrifuged, resuspended in freezing medium and
1022 stored in liquid nitrogen.
1023 Frozen cells were thawed at 37°C, followed by dropwise addition of 1 mL complete media (RPMI,
1024 10% Fetal bovine serum, 100 U/mL penicillin, 100 µg/mL streptomycin). Four Equivolume additions of
1025 complete media was added dropwise with gentle mixing in between additions for a total volume of 32
1026 mL. Thawed cells were washed twice with 4°C 1xDPBS and transferred to 5 mL FACS tubes
1027 (ThermoFisher). Live/dead stain was added, followed by a blocking buffer to bring samples to 0.5%
1028 BSA, 5% TruStain FcX buffer (BioLegend), 100 nM dasatinib, and control tetramers (oligo-PE-
1029 GSTDL594 and APCDL755-GST). Samples were then incubated on ice for 10 min followed by the
1030 following reagents in order: tetramers (T-Ag PE-oligo tetramer, T-Ag APC tetramer, RSV F PE-oligo
1031 tetramer, and RSV F APC tetramer), oligo-hashtag antibodies to identify sample origin in subsequent
1032 pooling steps, fluorochrome-labeled antibodies, and oligo-labeled antibodies. Cells were then incubated
1033 on ice for 30 min and washed three times with sorting buffer. Cells were then sorted on an Aria II Cell
1034 sorter (BD Biosciences). After exclusion of cell debris, dead cells, PE/APC tetramer-binding $CD19^+$
1035 $CD3^-$ $CD56^-$ $PE594^-$ $APC755^-$ B cells, tetramer-negative B cells $CD19^+$ $CD3^-$ $CD56^-$ $PE594^-$ $APC755^-$
1036 B cells, $CD3^+$ $CD19^-$ $CD56^-$ T cells, and $CD56^+$ $CD3^-$ $CD19^-$ cells were sorted into cold complete
1037 media, pooled and immediately prepared for sequencing. For most experiments, $tetramer^+$ $CD19^+$ B
1038 cells were sorted into a tube with $CD3^+$ T cells and kept separate from $Tetramer^-$ $CD19^+$ B cells that
1039 were sorted into a tube with $CD56^+$ MCC cells.
1040
1041 Single cell RNA-sequencing
1042 Single cell suspensions sorted from tumors and brought to a concentration of 700-1,200 cells/mL,
1043 loaded into microfluidic chip G (10X Genomics), and run through a Chromium controller to obtain Gel
1044 Beads-in-Emulsion (10X Genomics). Resulting cell suspensions then went through a library preparation
1045 process for single-cell RNA-sequencing along with paired V(D)J-seq for BCR and TCR receptor
1046 clonotypes using the 5' transcriptome kit with feature barcoding (V2; 10X Genomics) per manufacturer
1047 guidelines. The cDNA library was enriched for 1056 human immunology panel genes (10X Genomics)
1048 and sequenced using a NovaSeq instrument (Illumina) with 2 x 92 base pair paired-end reads aiming
1049 for an average of 20,000 reads/cell.
1050

1051 Single-cell RNA-sequencing data analysis
1052 Raw sequencing reads were aligned to the hg38 genome using Cell Ranger v.8.0.1. Filtered counts
1053 matrices of transcripts and feature barcoding counts were loaded into a SingleCellExperiment object for
1054 further analyses in R (v.4.1.2). Sample hash deconvolution was performed using DropletUtils (v.1.14.2).
1055 Doublets were detected using scds (v.1.10.0) and hash deconvolution and subsequently removed.
1056 Cells from different runs were then integrated using the mutual nearest neighbor method though the
1057 batchelor package (v1.10.0). UMAP dimensionality reduction was performed using the integrated
1058 values. Clustering was performed using the integrated transcript values reads through the walktrap
1059 algorithm on a nearest neighbor graph (scran v.1.22.1). Numbers of clusters was varied by scaling the
1060 number of nearest neighbors (k) during graph construction followed by analysis via clustree (v.0.5.0).
1061 Clusters were then labeled as major cell lineages of T cells, B cells, myeloid cells, epithelial cells,
1062 dendritic cells, and tumor cells through expression of key genes including *CD79A, CLEC4C, COL3A1,*
1063 *NCAM1, CD14,* and *CD3E*. Cluster labels were then validated by investigating the portion of cluster
1064 with productive BCR or TCR rearrangements. Cell lineages were then isolated *in silico* and
1065 dimensionality reduction and B cells re-clustered as above. Clusters were labeled based on expression
1066 of lineage markers (**Figure 3b**).
1067 To identify T-Ag-specific B cells in tumors, we analyzed T-Ag oligo reads and control antigen oligo
1068 reads in B cells. T-Ag-specific $CD19^+$ B cells were defined as cells with T-Ag oligo reads at least one
1069 log higher than background and fewer than 20 reads from GST or RSV F control antigens. Additionally,
1070 eight B cell families in which fewer than 50% of clones met this threshold were classified as non-
1071 specific. Sequences from tested antibodies were obtained from BCR sequencing analyses and are
1072 reported in **Table S10**.
1073
1074 BCR sequencing analysis
1075 Raw output files were demultiplexed and processed using CellRanger v.8.0.1 software (10X
1076 Genomics). For each donor, publicly available reference sequences from the IMGT/V-QUEST
1077 reference directory at https://www.imgt.org/ were used to identify V, D, and J gene segments. Next,
1078 data were processed and analyzed using the Immcantation Framework (http://immcantation.org) with
1079 Change-O v.1.0.2. For each 10X dataset, the filtered_contig.fasta file was annotated using IgBlast
1080 v.1.16 with the related donor-specific VJ genes database. To generate adaptive immune receptor
1081 repertoire (AIRR) rearrangement data, the filtered_contig_annotations.csv file was used, and only
1082 productive sequences were kept. The heavy and light chain sequences were separated in two files. The
1083 threshold for trimming the hierarchical clustering of B cell clones was determined by the SHazaM
1084 module for determining distance to nearest neighbor. With the Change-O DefineClones function, clones
1085 were assigned based on IGHV genes, IGHJ gene and junction distance calculated by SHazaM
1086 (distance 0.14). The generated clone-pass file was verified and corrected using the Change-O
1087 light_cluster function, based on the analysis of the light chain partners associated with the heavy chain
1088 clone. Independent clone-pass files were generated for each 10X run. For downstream analysis, all
1089 clone-pass files from were combined and re-clustered all together. Germlines were reconstructed using
1090 the Change-O CreateGermlines function. To obtain the final AIRR format file containing paired
1091 information on the same row, we used a Java script to process and filter the sequences. Only the heavy
1092 chains paired with one κ and/or one λ were filtered in for downstream analysis. Number and frequency
1093 of IgH mutations for each b cell were obtained using the SHazaM observedMutations function. Clonal
1094 families were visualized using the R package ggalluvial.
1095
1096 Multiplex immunohistochemistry of MCC tumors
1097 Formalin-fixed paraffin-embedded tissues were stained on a Leica BOND Rx autostainer using the
1098 Akoya Opal Multiplex IHC assay (Akoya Biosciences) with the following changes: Additional high
1099 stringency washes were performed after the secondary antibody and Opal fluor applications using high-
1100 salt TBST (0.05M Tris, 0.3M NaCl, and 0.1% Tween-20, pH 7.2-7.6). TCT was used as the blocking
1101 buffer (0.05M Tris, 0.15M NaCl, 0.25% Casein, 0.1% Tween 20, pH 7.6 +/- 0.1). Primary antibodies
1102 were incubated for 1 hour at room temperature. Tissues were counterstained with DAPI to identify the
1103 nuclei.

1104 Slides were mounted with ProLong Gold and cured for 24 hours at room temperature in the dark
1105 before image acquisition at 20x magnification on the Akoya PhenoImager HT Automated Imaging
1106 System. Images were spectrally unmixed using Akoya inForm software.
1107
1108 Multiplex immunohistochemistry image analysis
1109 HALO software (Indica Labs) High-Plex FL module was used to analyze each TMA slide image.
1110 Annotations of tumor and stroma sections were performed by a licensed pathologist. Cells were then
1111 identified based on the DAPI nuclear stain, and mean pixel fluorescence intensity was measured in
1112 applicable compartments for each cell. To account for variability across the TMA, cell detection
1113 algorithms were optimized individually for each TMA core to ensure accuracy. While many cores
1114 ultimately shared the same algorithm parameters, each core was initially assessed independently to
1115 determine the most appropriate settings using real-time tuning. The final algorithm parameters for each
1116 core were then applied accordingly. Two layers of quality control were performed: 1) comparing positive
1117 cell signals to positive object data results on at least six different cores, and 2) comparing cell counts to
1118 slide images reviewed by a pathologist. Summary data were exported to CSV files, and cell counts
1119 were merged with corresponding patient metadata using STATA 16. GraphPad PRISM 9 and R version
1120 4.2.1 (R Foundation for Statistical Computing) were used to generate plots and compare patient
1121 treatment groups.
1122
1123 TCR analysis and lentiviral expression in primary $CD4^+$ T cells
1124 TCR analysis was performed using some functions from Scirpy to assess clonal expansion and
1125 calculate clonotype size as previously described[37]. For TCR construction, the PRRL vector was
1126 modified with six start codon a promoter point mutations and cysteines were introduced to mediate TCR
1127 pairing as previously described[37]. TCR constructs were synthesized and sequence verified (Twist)
1128 containing codon-optimized DNA fragments of *TRBV*-*CDR3*-TRBJ-*TRBC* followed by a P2A skip
1129 sequence, TRAV-CDR3-TRAJ-TRAC cloned into PRRL-SIN. Lentivirus was produced freshly for each
1130 experiment. For this, Lenti-X cells (Clontech) were transiently transfected with each TCR vector and
1131 psPAX2 (Addgene plasmid no. 12260) and pCMV-VSV-G (Addgene plasmid no. 8454) packaging
1132 plasmids. Two days later, lentiviral supernatant was harvested from Lenti-X cultures, filtered using 0.45-
1133 mm polyethersulfone (PES) syringe filters (Millipore), and added to stimulated $CD4^+$ T cells in a 48-well
1134 tissue culture plate.
1135 For T cell transduction, $CD4^+$ T cells from control PBMC were thawed and stimulated with anti-
1136 CD3/anti-CD28 microbeads at a 3:1 bead:cell ratio (Dynabeads, Invitrogen) in T cell media containing
1137 L-glutamine and HEPES (Gibco) supplemented with 10% human serum, 50 mM beta-mercaptoethanol,
1138 penicillin, streptomycin, 4 mM L-glutamine, 50 U/mL IL-2, and 5 ng/mL IL-7 in RPMI for 2 days. On day
1139 2, magnetic beads were removed, and cells were nucleofected using a Lonza 4D nucleofector in 100
1140 mL of buffer P3 using program EH-115. TCR was knocked out using CRISPR targeting the first exon of
1141 the *TRBC* and *TRAC* alone as previously described[37]. For this, 80 mmol/L *TRAC* RNA (IDT), 80 mmol/L
1142 *TRBC* RNA (IDT), and 80 mmol/L of the gRNA AGAGTCTCTCAGCTGGTACA in duplex buffer (IDT),
1143 were mixed well and incubating in a heating block at 95ºC for 5 minutes followed by slowly cooling to
1144 room temperature. The resulting 40 mmol/L duplexed RNA was mixed with an equal volume of 24
1145 mmol/L Cas9 (IDT) and 1/20th volume of 400 mmol/L Cas9 electroporation enhancer (IDT) and
1146 incubated at room temperature for 15 minutes prior to nucleofection. Cells were allowed to rest for 4
1147 hours in media prior to lentiviral transduction. Polybrene (Millipore) was added to a final concentration
1148 of 4.4 mg/mL, and cells were centrifuged at 800 x *g* and 32ºC for 90 minutes. Sixteen hours later, viral
1149 supernatant was replaced with fresh T cell media. Half of the media was removed and replaced with
1150 fresh T cell media every 48 to 72 hours. Transduction efficiency into TCR knockout T cells was
1151 determined one week after nucleofection by measuring CD3 expression in each transduced sample
1152 compared to TCR knockout control T cells.
1153
1154 CRISPR engineering of B cells
1155 B cells were engineered to express T-Ag-specific antibodies as described previously[38]. Briefly,
1156 human B cell medium was IMDM supplemented with 10% FBS (Gemini Biosciences or Peak serum),

1157 100 U/mL penicillin and 100 µg/mL streptomycin (Gibco), except in antibiotic free steps as noted. Blood
1158 was obtained from adult volunteers by venipuncture and was approved by the Fred Hutch Institutional
1159 Review Board. Informed consent was obtained before enrollment. PBMCs were isolated from whole
1160 blood using Accuspin System Histopaque-1077 (Sigma-Aldrich) resuspended in 10% dimethylsulfoxide
1161 in heat-inactivated fetal bovine serum and cryopreserved in liquid nitrogen before use. PBMCs were
1162 thawed and B cells isolated using negative selection using the Human B Cell Isolation Kit II (Miltenyi)
1163 according to the manufacturer's recommendations. Isolated B cells were resuspended at $0.5\text{-}1.0\times10^6$
1164 cells/mL in stimulation media, which consisted of human B cell medium supplemented with 100 ng/mL
1165 MEGACD40L (Enzo Life Sciences), 50 ng/mL recombinant IL-2 (BioLegend), 50 ng/mL IL-10
1166 (Shenandoah Biotech), 10 ng/mL IL-15 (Shenandoah Biotech), 1 µg/mL CpG ODN 2006 (IDT) and
1167 incubated . After 48 hours, cells were electroporated using the Neon Transfection System. Cas9
1168 (Invitrogen) and gRNA (Synthego) were precomplexed at a 1 to 2 molar ratio in Neon Buffer T for 20
1169 minutes at room temperature. Cells were washed with 1xDPBS and resuspended to 2.5×10^7 cells/mL in
1170 Neon Buffer T containing 12 µg of precomplexed gRNA/Cas9 per 10^6 cells. The cell/huIgH$_{296}$
1171 gRNA/Cas9 mixture was electroporated with one 20 millisecond pulse at 1750V and immediately plated
1172 into stimulation media as described above, without antibiotics. After 30 minutes, AAV was added to a
1173 final concentration of up to 20% culture volume amounting to a MOI of $10^5\text{-}10^6$ genome copies per cell
1174 and incubated for 2 - 4 hours. AAVs were produced by VectorBuilder containing an equimolar
1175 concentration of antibody constructs corresponding to 1G04, 2H04, and 1B09 from containing the full
1176 antibody light chains physically linked to the heavy chain VDJs with a linker[39] containing Strep-tagII[40-42].
1177 Cells were next transferred to a larger culture dish to allow for further expansion for two days. For
1178 secondary expansion, every four days B cells were passaged onto irradiated (80 gy) NIH 3T3-CD40L
1179 feeder cells in human B cell medium containing 5 µg/mL human recombinant insulin (Sigma), 50 µg/mL
1180 transferrin (Sigma), 50 ng/mL human IL-2 (BioLegend), 20 ng/mL human IL-21 (BioLegend), and 10
1181 ng/mL human IL-15 (Shenandoah Biotech).
1182
1183 Stimulation of T-Ag-specific CD4$^+$ T cells by B cells
1184 Engineered or control B cells from the same donor as T cells were isolated from thawed PBMC by
1185 positive selection using human CD19 microbeads (Miltenyi) according to the manufacturer's
1186 instructions. Isolated B cells were cultured with irradiated (5000Gy) NIH 3T3 cells expressing human
1187 CD40L in B cell medium supplemented with 200 U/ml human IL-4 (Peprotech). B cells were harvested
1188 and restimulated with 3T3 CD40L every 7 days and supplemented with fresh medium and cytokines
1189 every 3 days. For tumor lysate preparation, WaGa tumor cells were counted and resuspended at
1190 $5\text{x}10^6$/mL in serum free RPMI media. Cell suspension was frozen/thawed 5 times alternating between
1191 three minutes submerged in liquid nitrogen and three minutes in a 37 ^{o}C water bath. Solution was then
1192 centrifuged for 5 minutes at 1000 x G to remove debris and remaining cells. Supernatant was then
1193 transferred to a fresh tube to be used as tumor lysate. 25 µL lysate was added to co-cultures for a total
1194 volume of 200µL per well. 10^5 B cells were mixed with 50,000 transduced T cells in the presence or
1195 absence of 0.1 or 5 mg/mL of T-Ag peptide pools, 0.1 - 10 mg/mL of purified T-Ag, or crude lysate
1196 derived from WaGa MCC cells for 24 hours prior to detection of IFNγ in culture supernatant using the
1197 using an ELISA kit (ThermoFisher). Alternatively, the expression of OX40 and CD40L was measured
1198 using flow cytometry.
1199
1200 Quantification and statistical analysis
1201 The statistical tests applied were two-sided unless specified otherwise. T tests were used to
1202 compare differences between two groups unless otherwise noted. When comparing more than two
1203 groups, the nonparametric Kruskal–Wallis test was used. Fisher's exact test was used to evaluate
1204 differences between two categorical variables. The significance levels for Kaplan–Meier analyses were
1205 calculated using a two-sided log rank test. GraphPad Prism 9 and R version 4.2+ (R Foundation for
1206 Statistical Computing) were used to generate plots and compare patient treatment groups.